The Journal of Comparative Neurology 517:105–121 (2009)
Research in Systems Neuroscience

Drebrin A Knockout Eliminates the Rapid Form of Homeostatic Synaptic Plasticity at Excitatory Synapses of Intact Adult Cerebral Cortex

CHIYE AOKI,[1]* NOBUHIKO KOJIMA,[2] NICOLE SABALIAUSKAS,[1,3,4] LOKESH SHAH,[1] TUNAZZINA H. AHMED,[1] JOHN OAKFORD,[1] TAHIR AHMED,[1] HIROYUKI YAMAZAKI,[2] KENJI HANAMURA,[2] AND TOMOAKI SHIRAO[2]

[1]Center for Neural Science, New York University, New York, New York 10003
[2]Department of Neurobiology and Behavior, Gunma University Graduate School of Medicine, Maebashi, Gunma, 371-8511 Japan
[3]Sackler Institute for Biomedical Sciences, New York University Langone Medical Center, New York, New York 10016
[4]Department of Pharmacology and Physiology, SUNY Downstate Medical Center, Brooklyn, New York 11203

ABSTRACT

Homeostatic synaptic plasticity (HSP) is important for maintaining neurons' excitability within the dynamic range and for protecting neurons from unconstrained long-term potentiation that can cause breakdown of synapse specificity (Turrigiano [2008] Cell 135:422–435). Knowledge of the molecular mechanism underlying this phenomenon remains incomplete, especially for the rapid form of HSP. To test whether HSP in adulthood depends on an F-actin binding protein, drebrin A, mice deleted of the adult isoform of drebrin (DAKO) but retaining the embryonic isoform (drebrin E) were generated. HSP was assayed by determining whether the NR2A subunit of N-methyl-D-aspartate receptors (NMDARs) can rise rapidly within spines following the application of an NMDAR antagonist, D-APV, onto the cortical surface. Electron microscopic immunocytochemistry revealed that, as expected, the D-APV treatment of wild-type (WT) mouse cortex increased the proportion of NR2A-immunolabeled spines within 30 minutes relative to basal levels in hemispheres treated with an inactive enantiomer, L-APV. This difference was significant at the postsynaptic membrane and postsynaptic density (i.e., synaptic junction) as well as at nonsynaptic sites within spines and was not accompanied by spine size changes. In contrast, the D-APV treatment of DAKO brains did not augment NR2A labeling within the spine cytoplasm or at the synaptic junction, even though basal levels of NR2A were not significantly different from those of WT cortices. These findings indicate that drebrin A is required for the rapid (<30 minutes) form of HSP at excitatory synapses of adult cortices, whereas drebrin E is sufficient for maintaining basal NR2A levels within spines. J. Comp. Neurol. 517: 105–121, 2009. © 2009 Wiley-Liss, Inc.

Indexing terms: homeostatic synaptic plasticity; synaptic plasticity; drebrin A

Neurons throughout the CNS are endowed with mechanisms that integrate activity over time and convert these into signals that regulate the maintenance and upward/downward changes in the expression of genes encoding receptors and channels. Some of the mechanisms underlying this self-regulation are achieved locally and rapidly at synapses (Malenka and Bear, 2004; Perez-Otano and Ehlers, 2005). Without these checks and balances, steady maintenance of synaptic strength (homeostatic synaptic plasticity) is lost, and this could lead to unconstrained long-term potentiation (LTP), excessive excitation of neurons, and degradation of synapse specificity (Turrigiano, 2008).

In cortex and hippocampus, excitatory synapses form almost exclusively at spines, a specialized structure, typically less than 1 μm in diameter, where glutamate receptors and their scaffolding proteins and signaling molecules, such as αCaMKII, are organized (Kennedy and Ehlers, 2006). Through quantitative electron microscopic-immunocytochemistry (EM-ICC), we have demonstrated that spines of adult rat cortex can respond rapidly (<30 minutes) to blockade of N-methyl-D-aspartate receptors (NMDAR) by increasing the levels of the NMDAR subunit NR2A, precisely at axospinous synaptic junctions and within the spine

Grant sponsor: National Institutes of Health; Grant number: 1 P30 EY13079; Grant number: 5 R01 DA009618-09; Grant number: R01 NS41091; Grant number: R01 13145; Grant sponsor: NYU Research Challenge Fund; Grant sponsor: National Science Foundation-REU (to C.A.); Grant sponsor: Ministry of Education, Culture, Sports, Science and Technology of Japan; Grant number: 19200029; Grant number: 20021002.

John Oakford's current address is University of Rochester, Rochester, NY 14627. Tahir Ahmed's current address is Stroke Branch, NINDS, Building 49, 49 Convent Drive, Bethesda, MD 20892. Lokesh Shah and John Oakford are in the Research Experience for Undergraduate Program at the Center for Neural Science, New York University.

*Correspondence to: Chiye Aoki, Center for Neural Science, New York University, New York, NY 10003. E-mail: ca3@nyu.edu

Received 28 January 2009; Revised 22 March 2009; Accepted 30 May 2009

DOI 10.1002/cne.22137

Published online June 11, 2009 in Wiley InterScience (www.interscience.wiley.com).

cytoplasm (Aoki et al., 2003). Such a response would be useful for returning excitability of NMDAR-antagonized synapses toward the original set point. This form of homeostatic synaptic plasticity was first observed for cultured hippocampal neurons (Rao and Craig, 1997), although the response observed there may have been more sluggish, insofar as NMDAR's NR1 puncta were reported to increase only after exposing neurons to D-APV for a minimum of 7 days. For any of these examples of activity-dependent plasticity, rapid or slower, our understanding of the molecular mechanisms underlying NMDAR insertion at synapses is incomplete. However, converging evidence indicates that receptor turnover at synapses involves the interaction of plasmalemmal mechanisms to capture receptors at synapses and the cytoplasmic organelles that deliver receptor cargos into and out of spines and to the postsynaptic membrane (Groc and Choquet, 2006; Kennedy and Ehlers, 2006; Perez-Otano and Ehlers, 2005). These studies exploring the molecular mechanisms underlying plasticity of excitatory synapses indicate that F-actin plays a central role, in that both the synaptic capturing and translocation of receptor cargos to synapses involve F-actin (Allison et al., 1998, 2000; Halpain, 2006; Halpain et al., 1998; Kennedy and Ehlers, 2006; Krupp et al., 1999; Star et al., 2002; Wyszynski et al., 1997). These observations suggest that candidate molecules linking synaptic activity to receptor localization are likely to be enriched at the postsynaptic side of excitatory synapses and to exhibit F-actin-binding characteristics.

More recently, we showed that the increase of NR2A in dendritic spines is accompanied by increases of F-actin and an F-actin binding protein, drebrin A (Fujisawa et al., 2006). Drebrin A is the only neuron-specific, F-actin binding protein that is found exclusively on the postsynaptic side of excitatory synapses (Aoki et al., 2005). In that study, we were prompted to examine whether synaptic activity regulates the localization of drebrin A within spines, because a number of studies (Shirao and Sekino, 2001) had indicated that drebrin [the embryonic (E) or adult (A) isoforms] has properties suitable for modulating the trafficking of proteins into and out of spines as well as modifying the shape and even the stability of spines. One of drebrin's interesting properties is to reduce the sliding velocity of actin filaments on immobilized myosin and inhibit the actin-activated ATPase activity of myosin (Hayashi et al., 1996). Such a property could underlie drebrin's ability to regulate the accumulation of synaptic molecules within spines. Because drebrin can bind to F-actin, it can displace α-actinin's binding to F-actin and, in this way, also liberate the link between NMDARs and F-actin (Shirao and Sekino, 2001). If drebrin resides precisely at the synapse, this property could help in unloading receptors at the postsynaptic membrane and also liberate NMDARs that are tethered to the subsynaptic F-actin lattice. By displacing α-actinin from F-actin, drebrin can also make F-actin accessible to gelsolin. Gelsolin, in turn, severs F-actin into shorter fragments in a calcium-dependent manner (Kinosian et al., 1998), and this action may alter the fluidity of the cytoplasm, thereby facilitating the diffusion of cytoplasmic organelles and proteins into, out of, and within the spine cytoplasm. In accordance with both of these properties that are linked to the displacement of α-actinin, drebrin A knock-down of cultured hippocampal neurons by antisense treatment leads to impairment in the NMDAR-blockade-evoked up-regulation of the NR1 subunits within spines (Takahashi et al., 2006). The action of gelsolin upon F-actin, which is promoted by the presence of drebrin, can also increase spine shape flexibility. Indeed, knock-down of drebrin within cultured hippocampal neurons by RNAi promotes stabilization of dendritic protrusions, leading to an increased population of globular, mature, stable spines in an F-actin/Ras-dependent manner (Biou et al., 2008).

Although these studies indicate that drebrin is an excellent candidate for linking NMDAR activity to NMDAR localization at synapses, all of these experiments were performed using acellular systems or hippocampal neurons grown in vitro. Thus, whether drebrin A exerts activity-dependent regulation on the redistributions of receptors within intact tissue and, especially, in fully mature brains has yet to be tested. Nevertheless, this question is important, because drebrin is one protein that declines in brains of patients diagnosed with Alzhemier's disease or mild cognitive impairment (Counts et al., 2006; Harigaya et al., 1996; Hatanpaa et al., 1999; Shim and Lubec, 2002) and in animal models of Alzhemier's disease (Aoki et al., 2007; Calon et al., 2004) in the early stages (Aoki et al., 2007; Calon et al., 2004).

The in vitro pharmacological manipulations described above rendered the spine shapes less stable, thereby precluding analysis of receptor redistribution separately from spine shape stability. Moreover, without the use of EM, the distinction of receptor immunoreactivity precisely at the surface vs. nonsurface portions of the spine is difficult, particularly for neurons within intact tissue. Therefore, in the current study, we examined the impact of knockout of the adult isoform of drebrin (drebrin A) on the responsiveness of spines to NMDAR blockade. Drebrin A knockout (DAKO) mice were generated by targeted knockout of exon 11A, encoding the drebrin A specific insertion. These animals continue to express the embryonic isoform, drebrin E, instead of switching to drebrin A in adulthood. We demonstrate that DAKO eliminates the rapid NMDAR blockade-evoked rise of NR2A levels within spines and at the postsynaptic density (PSD), even though resting levels of NR2A at the postsynaptic membrane are comparable to the levels observed within control hemispheres of age-matched wild-type (WT) animals. These observations indicate that drebrin A is required for homeostatic synaptic plasticity, whereas drebrin E is sufficient for maintaining adult levels of NR2A at postsynaptic membranes. Moreover, the rapidity with which spines respond, in the presence of drebrin A, indicates that spines of intact neurons possess the mechanism to regulate receptor levels at synapses without evoking transcriptional mechanisms.

MATERIALS AND METHODS

Generation of DAKO mice

All DAKO mice and WT littermates were bred at the animal facility of Gunma University Graduate School of Medicine, Gunma, Japan, in accordance with the guidelines published in the NIH *Guide for the care and use of laboratory animals* and Gunma University's Animal Care and Experimentation Committee. All ante mortem experiments were carried out according to the Animal Care and Experimentation Committee of Gunma University, Showa Campus, and of NYU's University Animal Welfare Committee.

All mice were F4-generation adult male. DAKO mice were generated by targeted knockout of exon 11A, encoding the

drebrin A-specific insertion, whereas control animals were 11A homozygous WT (+/+). An outline of the procedure for generating DAKO mice is presented here, but a more complete description appears elsewhere (Kojima et al., manuscript in preparaption). Briefly, a rat drebrin A cDNA (clone Drh102; Shirao et al., 1992) was used as the probe for screening the C57BL/6 mouse genomic DNA BAC library (BACPAC Resources Center, Oakland, CA) for the drebrin gene. From one of these BAC clones, DNA fragments covering the genomic locus containing exon 11A were subcloned and characterized. For construction of the targeting vector, exon 11A, encoding the drebrin A-specific insertion (ins2; Jin et al., 2002), was flanked by loxP sites (Sternberg and Hamilton, 1981). For the positive and negative selections, the PGK-neo cassette (Wu et al., 1994) flanked by frt sites (Broach et al., 1982) and the pMC1DT-A were inserted into the 3′ direction of exon 11A and the 5′ end of the targeting vector, respectively. This construct was linearized and electroporated into C57BL/6 mouse embryonic stem (ES) cells (line MS12; Kawase et al., 1994) as described previously (Homanics et al., 1997). The recombinant ES clones were screened by Southern blot analysis. ES cell clones that harbored the targeted locus were injected into C57BL/6 blastocysts to produce chimeric mice. Chimeric animals were mated with C57BL/6 females to establish germline transmission. Heterozygous (F/+) male mice of the F1 generation were subsequently mated with EIIa-Cre transgenic mice (Lakso et al., 1996) to delete the drebrin exon 11A flanked by loxP sites. Mice carrying the deletion of exon 11A were selected by PCR of the tail DNA. Mice heterozygous for the 11A null allele were back-crossed to C57BL/6 females for obtaining the breeder and intercrossed for obtaining mice homozygous for the 11A null allele (–/–). The KO homozygous mice continue to express the embryonic isoform, drebrin E, instead of switching to drebrin A in adulthood (Fig. 1).

DAKO and WT male mice were marked by ear punching at the Gunma University facility, to be able to identify each animal according to its ID number and genotype. At the age of 3 months, those animals to be used for light and electron microscopy and homeostatic synaptic plasticity assay were transported from Japan to the United States, via World Courier. The genotype of each animal was confirmed in three ways: by genotyping the DNA prior to shipping, by genotyping the DNA again after shipping, and by the EM-ICC detection of drebrin A within spines (Fig. 2). NYU investigators were kept blind regarding the genotype of the animals until all parts of the experimental procedure (surgery, immunocytochemistry, and EM quantification) were completed, to minimize any potential for the NYU team to be biased in their treatment of the animals or in the tissue sampling or the quantification procedure. Throughout the experimental procedures at NYU, the animals were referred to by new ID numbers: 5, 6, 7, 8, 9, 10, and 11, given in the United States, to conceal the genotype to all participating investigators at NYU except for one.

Antibody Information and chemicals

Information about the primary antibodies used in this study is given in Table 1. The anti-drebrin A antibody DAS2 was generated and characterized previously for its specificity (Aoki et al., 2005), based on elimination of immunoreactivity within whole-brain homogenates obtained from DAKO mice, as assessed by Western blotting, and recognition of a single band in homogenates from WT mouse brains at the expected molecular weight of 116 kD (Fig. 1). DAS2 is generated by using the immunogen Phe-Ile-Lys-Ala Ser-Asp-Ser-Gly-Pro-Ser-Ser-Ser, which corresponds to a sequence of residues 325–336 of drebrin that is unique to the adult form, drebrin A (Shirao et al., 1992). DAS2 was produced in rabbits, and purified by epitope selection, with the above-mentioned polypeptide. This antibody is able to discriminate drebrin A from its isomer, drebrin E, as shown in Figure 1. The pan-drebrin antibody was a mouse monoclonal antibody M2F6 produced using the protein, drebrin, that was purified electrophoretically from the soluble fraction of 11-day-old chick embryo brains (Shirao and Obata, 1986; Fig. 1), as the immunogen. By Western blotting, the pan-drebrin antibody recognizes two bands within whole-brain homogenates of WT mouse brains, corresponding to drebrin A and drebrin E (Fig. 1).

The anti-NR2A subunit antibody was purchased from Upstate Biotechnology (Lake Placid, NY, now part of Millipore; catalog No. 07-632, 1 mg/ml undiluted). The antibody was produced with a peptide corresponding to amino acids 1265–1464 of the C-terminus as the immunogen and was generated by immunizing rabbits. Specificity of this antibody has been demonstrated previously by Western blotting, which shows that this antibody recognizes a single band corresponding to the molecular weight, ~170 kD, of the NR2A subunit and neither the NR2B nor NR1 subunits of NMDAR (Rinaldi et al., 2007). Previously and currently conducted EM-ICC study from this laboratory determined that this antibody recognizes

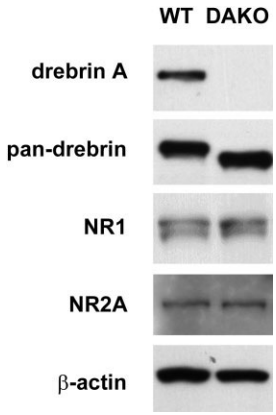

Figure 1.
Persistence of drebrin E and absence of drebrin A within adult DAKO brain homogenates. Whole homogenates of two adult WT and two adult DAKO cerebral cortices were analyzed for the presence of drebrin and NMDAR subunits by Western blotting. When probed using the drebrin A-specific antibody (DAS2), brain homogenates prepared from WT mice exhibited a single band corresponding to drebrin A. In contrast, the homogenate from DAKO mice exhibited no immunoreactive band. When probed using the monoclonal antibody that recognizes both embryonic and adult isoforms of drebrin (M2F6), the brain homogenate prepared from WT mice exhibited a band corresponding to drebrin A concomitantly with a faint band corresponding to drebrin E. In contrast, brain homogenate prepared from age-matched DAKO mice exhibited only a single band with apparent molecular weight corresponding to that of drebrin E. Western blots probed with anti-NR1 and anti-NR2A subunits of NMDARs and with anti-β-actin yielded identical bands in lanes loaded with WT and DAKO homogenates.

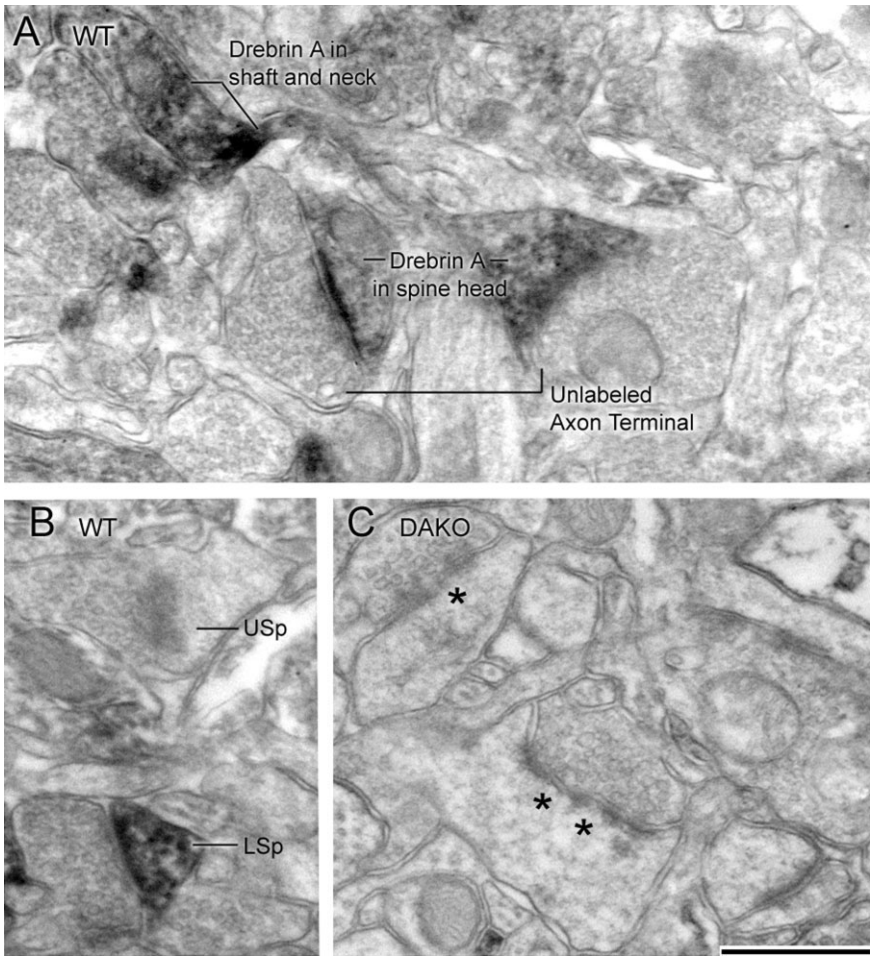

Figure 2.
Drebrin A immunolabeling within WT and DAKO cortices. EM-ICC was performed using the drebrin A-specific antibody DAS2. All panels show electron micrographs taken from layer 1 of the cerebral cortex. In the WT tissue, HRP-DAB immunolabeling is evident within the spine head, dendritic shaft, and portions of the spine neck (**A**). Within spine heads, the immunoreactivity can be diffuse (spine to the right in A), can occur concentrated at the postsynaptic density (PSD; spine to the left in A), or can be distributed throughout the spine cytoplasm and at PSDs (LSp in B). **B** also shows an example on an unlabeled spine head (USp). The DAKO tissue shown in **C** was processed in parallel to the tissues shown in A and B. Immunoreactivity is not detectable within spines. Asterisks indicate examples of interruptions in the PSDs, indicating that the PSDs are perforated. These samples were obtained by an investigator kept blind to the genotype of the animal. The collection of such micrographs was used to determine the frequency of drebrin A labeling within spines for the purpose of confirming the genotype of each animal. Scale bar = 500 nm.

asymmetric synapses but not the symmetric synapses (Kobayashi et al., 2007), thereby indicating synapse and pathway specificity in staining pattern generated by this antibody. The NR1 antibody was produced using an immunogen that was a fusion protein encoding the glutathione S-transferase frame with the amino acid sequence corresponding to residues 660–811 of the intracellular loop between putative transmembrane regions III and IV of the NR1 subunit of NMDARs. This is a mouse monoclonal antibody purchased from BD Biosciences (clone 54.1, catalog No. 56308; originally distributed by Pharmingen, 0.5 mg/ml undiluted). The NR1 antibody has been shown to be specific, based on reactivity to a single band of MW 120 kDa by Western blotting and the absence of reactivity to the NR2A subunit expressed in 293 cells [BD Sciences and Pharmingen's data sheets and previously described (Brose et al., 1994) findings]. Our previous EM study also showed that this antibody recognizes asymmetric (presumably excitatory) synapses, but not the symmetric (presumably inhibitory) synapses (Farb et al., 1995).

The β-actin antibody was a mouse monoclonal antibody purchased from Sigma (St. Louis, MO; clone AC-15, 1.5 mg/ml undiluted). This antibody has been shown to recognize a single band at the expected molecular weight of 42 kDa (manufacturer's data sheet). The immunogen was a slightly modified β-cytoplasmic actin N-terminal peptide, Ac-Asp-Asp-Asp-Ile-Ala-Ala-Leu-Val-Ile-Asp-Asn-Gly-Ser-Gly-Lys, conjugated to keyhole limpet hemocyanin (KLH).

Secondary antibodies were biotinylated goat anti-rabbit IgG (Vector's Elite kit; catalog No. PK-6200; Vector, Burlingame, CA) or gold-conjugated goat anti-rabbit IgG, where the colloidal golds were either 0.8 nm or 10 nm in diameter (Aurion, EM Sciences, Fort Washington, PA; catalog Nos. 800.011 and

TABLE 1. Primary Antibodies Used

Antigen	Immunogen	Manufacturer, species in which antibody was raised, mono- vs polyclonal, catalog or lot No.	Dilution used
NR2A subunit of NMDA receptors	Amino acids 1265-1464 of the C-terminus of mouse NR2A subunit	Upstate Biotechnology, (now Millipore, Billerica, MA), polyclonal antibody raised in rabbit, catalog No. 07-632	1 μg/ml for HRP-DAB; 10 μg/ml for postembed gold immunolabeling; 1:1,000 for Western blot
NR1 subunit of NMDA receptors	Amino acids 660-811	BD Biosciences Japan (originally Pharmingen), monoclonal antibody 54.1	1:2,000
β-Actin	Slightly modified β-cytoplasmic actin N-terminal peptide, Ac-Asp-Asp-Asp-Ile-Ala-Ala-Leu-Val-Ile-Asp-Asn-Gly-Ser-Gly-Lys, conjugated to KLH	Sigma-Aldrich Japan, monoclonal antibody AC-15	1:10,000
Drebrin A	Amino acid residues 325-336, which are unique to drebrin A and absent in drebrin E	DAS2, generated and provided by the Shirao laboratory, polyclonal antibody raised in rabbit	1:1,000 for EM-ICC; 1:500 for Western blot
Drebrin E	Whole drebrin protein purified from E11 chick embryos (Shirao and Obata, 1986)	M2F6, generated and provided by the Shirao laboratory, mouse monoclonal antibody	Undiluted supernatant

810.011, respectively). D- and L-APV and bovine serum albumin (BSA) were purchased from Sigma. Glutaraldehyde, osmium tetroxide, paraformaldehyde, and EMBED-812 were purchased from EM Sciences. The Silver IntesEM kit was purchased from Amersham (Arlington Herights, IL; now part of GE; catalog No. RPN 491).

NMDAR blockade

Homeostatic plasticity was tested in three DAKO and four WT mice. All were adult males ranging in age from 105 to 111 days postnatal. The animals received the NMDAR blocker D-APV unilaterally over the cerebral cortex, by using the procedure detailed previously (Aoki et al., 2003; Fujisawa and Aoki, 2003; Fujisawa et al., 2006) but with minor changes described here. All procedures were performed with aseptic techniques while maintaining the animal anesthetized with isoflurane (2–3%) and normothermic with a water-circulating heating pad. The NMDAR blocker D-aminophosphovaleric acid (D-APV; 5 mM) was delivered to the cortical surface of anesthetized mice for 30 minutes, immediately prior to euthanasia. The active enantiomer, D-APV, was delivered to the cortical surface of one hemisphere only, by first thinning a 1 mm × 3 mm skull region overlying the dorsal neocortex with a dental drill, then using forceps to lift the thinned disk of bone (~100 μm thick). The underlying dura was lifted, then nicked with a bent, sterile 28-guage hypodermic needle tip. Immediately thereafter, a piece of sterile gelfoam, small enough to fit inside the drilled hole, and soaking in sterile artificial cerebral spinal fluid (115 mM NaCl, 3.3 mM KCl, 1 mM $MgSO_4$, 2 mM $CaCl_2$, 25.5 mM $NaHCO_3$, 1.2 mM NaH_2PO_4, 5 mM lactic acid, and 25 mM glucose) containing 5 mM of D-APV was placed gently over the cortical surface. To deliver the control solution to the contralateral cortex, the skull overlying the contralateral cortical surface was removed similarly. Then, a piece of gelfoam soaked with 5 mM of L-APV, an inactive enantiomer, instead of D-APV was placed over the contralateral cortical surface. We have verified, based on results from previous studies, that the contralateral cortex treated with L-APV serves as the intraanimal control brain region, equivalent in NR2A levels to portions of the cortex receiving no drug treatment (Aoki et al., 2003; Fujisawa and Aoki, 2003; Fujisawa et al., 2006). The drug concentrations used, 5 mM, is one-tenth of the concentrations used most commonly for iontophoresis and long-term delivery of the drug with an osmotic minipump (Aguilar et al., 2003; Bear et al., 1990; Cline and Constantine-Paton, 1990; Malmierca and Nunez, 2004; Miller et al., 1989; Rabacchi et al., 1992).

Preparation of brain tissue for light and electron microscopy

At the end of the 30-min D/L-APV delivery, mice received a supplement of anesthetic, consisting of 50 mg/kg Nembutal i.p. Two to three minutes following i.p. delivery of supplement, the depth of anesthesia was ascertained by testing for reflex to increasing pinching pressure to the paw and light touch of the cornea. Transcardial perfusion was achieved by using a peristaltic pump to control the flow rate of the perfusates. The perfusates were the following: 1) 10–50 ml of saline containing heparin (1,000 U/ml), delivered for 1 minute at a flow rate of 50 ml/minute; 2) 200 ml of 0.10% glutaraldehyde, mixed with 4% paraformaldehyde in 0.1 M phosphate buffer (pH 7.4), delivered at a flow rate of 50 ml/minute during the initial 1 minute, then slowed to a rate of 15 ml/minute during the subsequent 10 minutes. During the subsequent hours, the brain was cut into 40-μm-thick sections using a vibratome. In the fifth hour following the perfusion, the sections were immersed in PBS containing 1% sodium borohydride, to terminate residual cross-linking activities of glutaraldehyde with precise timing. Subsequently, the sections were stored for up to 1 month free-floating at 4°C in PBS containing 0.05% sodium azide.

Two DAKO and one WT animal that did not receive NMDAR blockade were also perfused transcardially with aldehydes for morphological analyses only. These sections did not undergo ICC procedures and were postfixed with 1% osmium tetroxide.

NR2A immunocytochemistry and the rationale for the choice of the three immunolabels

Immunocytochemistry was performed to immunolabel the NR2A subunits of NMDAR, with three immunolabeling procedures for EM. The three immunolabels we employed were horseradish peroxidase/3,3′-diaminobenzidine (HRP-DAB), silver-intensified immunogold (SIG), and postembed immunogold (PEG). HRP-DAB was employed because the enzymatic amplification step allows for the lowest threshold for detection. However, the enzymatic amplification also generates a diffusible label, and this causes degradation of the information regarding the precise localization of the antigen within spines. SIG complements HRP-DAB by providing better localization, but at the expense of high threshold for detection. With both HRP-DAB and SIG, antigens residing directly over the PSDs can be difficult to detect, because of the heavy matrix of proteins surrounding the synaptic cleft that interferes with antibody access. The PEG approach complemented the HRP-

DAB and SIG approaches for localizing antigens over the PSD, although some of the antigens might have been lost during EM tissue processing. Because of these known advantages and shortcomings of each EM immunolabel, we opted to test the NR2A levels with all three procedures. Details of the ICC procedures were as described previously (Aoki et al., 2000), with slight modifications as described recently (Sarro et al., 2008).

Two of the immunolabels were applied on free-floating sections prior to embedding in the resin EM812. One was HRP, using 3,3′-diaminobenzidine and H_2O_2 as substrates (HRP-DAB), to optimize detection of immunolabels within spines. The second was silver-intensified 0.8-nm colloidal gold (SIG) conjugated to secondary antibodies (1:100). Although the SIG procedure is less sensitive than the enzymatically amplified HRP-DAB, the SIG procedure was employed to identify the location of antigens at synaptic vs. nonsynaptic sites within spines. These preembedding procedures employed the NR2A antibody at a concentration of 1 μg/ml, incubated overnight at room temperature under constant agitation. The HRP-DAB-labeled sections were postfixed with 1% osmium tetroxide. The SIG-labeled sections were postfixed by using Phend's procedure, which excludes fixation with osmium tetroxide (Phend et al., 1995), to protect the SIG particles from oxidation. The third immunolabel was PEG. Although antigenicity is frequently lost during the EM procedures required for plastic embedding, the ultrathin sectioning step can also reveal antigens that are embedded within large proteinaceous matrix, such as the PSD. The PEG method was used to quantify the level of NR2A immunolabels positioned directly over the PSD. The concentration of the NR2A antibody used for the PEG procedure was 10 μg/ml, incubated overnight at room temperature. The PEG procedure employed anti-rabbit IgG antibodies (1:100) conjugated to 10-nm colloidal gold. For the PEG procedure, ultrathin sections were collected on formvar-coated, 200-mesh EM grids and following Phend's general procedure for PEG labeling, with vibratome sections that were fixed in the absence of osmium tetroxide (Phend et al., 1995), with modifications described specifically for PEG labeling of NR2A subunits (Erisir and Harris, 2003).

Drebrin A immunocytochemistry

Drebrin A immunocytochemistry was achieved by using the drebrin A antibody DAS2 at a concentration of 1:1,000, incubation overnight at room temperature, and HRP-DAB as the immunolabel. Tissue was postfixed with osmium tetroxide and processed for EM as described previously (Aoki et al., 2005).

ICC controls

Besides the Western blotting controls described under Antibody information and chemicals, each of the three EM-ICC procedures was accompanied by ICC controls. These consisted of verifications that omission of the primary antibody or use of secondary antibodies that were mismatched for species yielded no immunolabeling that could be detected by light or electron microscopy. In addition, EM examination revealed that neither the NR2A nor the drebrin A immunolabeling occurred postsynaptic to symmetric (presumably inhibitory) synapses, thereby indicating specificity of labeling at the subsynaptic level and in a pathway-specific manner, as described previously (Aoki et al., 2005; Erisir and Harris, 2003).

Image capture and areas sampled for EM

The person capturing the images was kept blind to the genotype and pharmacological treatment that the animal received, to eliminate bias in the sampling of neuropil. Images used for quantitative analyses were captured digitally with a Hamamatsu CCD camera attached to a JEOL 1200XL EM and software developed by AMT, Inc. (Boston, MA). Adjustments to the images, including size, brightness, and contrast, were carried out in Adobe Photoshop 7.0 (Adobe, San Jose, CA) to optimize discrimination of immunolabel from postsynaptic densities.

The images were taken at a magnification of ×40,000, with each digitized frame spanning 29 μm^2 of area. Systematic sweeps were made across the tissue, to avoid capturing the same field more than once. Micrographs used for quantitative analyses were taken from regions of the neuropil that fulfilled the following criteria. 1) The neuropil resided in layer 1 of the cortex, where penetration of the drug, D/L-APV, that was applied from the cortical surface into the underlying neuropil would be maximal (Aoki et al., 2003). 2) For the HRP-DAB- and SIG-labeled tissue, the neuropil resided within portions of vibratome sections forming the razor-blade-cut surface, where penetration of immunoreagents into the vibratome sections would be maximal. 3) The synaptic neuropil was free of ultrastructural features reflective of trauma associated with surgery, such as swollen mitochondria, swollen neurites, and/or electron-dense cytoplasm. The fields shown in Figures 2–4 and 6 are examples of ultrastructure that were deemed satisfactory for use in quantitative analysis, insofar as they fulfilled all three of the criteria.

Quantitative EM analyses

For all parts of the quantitative analysis, the person performing the tallying was kept blind to the genotype and pharmacological treatment of the animal. Within two-dimensional, digitized image frames, synapses were identified as excitatory, based on the presence of thick PSD that aligned the intracellular surfaces of plasma membranes abutting vesicle-filled axon terminals. Excitatory synapses were numbered in the order encountered. Each excitatory synapse was subsequently categorized as being associated with or without NR2A or drebrin A immunolabel. At minimum, 100 synapses and in most cases more than 200 synapses were sampled from each hemisphere of each animal. For every group of 10 synapses encountered, the number of synapses associated with immunolabel was tallied. This tallying was repeated 10–20 times for each hemisphere of each cortical hemisphere, and the mean and SEM of the percentage of synapses associated with label was calculated for each hemisphere.

For HRP-DAB- and especially for the SIG- and PEG-labeled tissue, the immunolabeling was sufficiently discrete to allow discrimination of the immunoreactive sites as contiguous or not contiguous with the postsynaptic specialization. For quantification of SIG-labeled tissue, the position of the immunolabel was categorized further as being "at or near the postsynaptic membrane," if the center of any of the SIG cluster was found directly over the PSD or within a distance equal to the thickness of the PSD in its plane of section. For PEG-labeled tissue, the position of immunolabel was categorized as being at or near the PSD, if the immunolabeling was directly over the PSD ("at PSD"), within a distance equal to the thick-

TABLE 2. Morphology of Synapses in Layer 1 of WT and DAKO Cortices

	WT	DAKO	*P* value
Encounter with synapse profile (per micrograph of area 29 μm^2; n is number of micrographs)	5.34 ± 0.18 (n = 142)	5.13 ± 0.18 (n = 143)	0.398
Synapse density, per 10 μm^3 estimated by using Abercrombie's correction	5.58 ± 0.19	5.35 ± 0.19	
Freq. of perforated synapses (% of 2,770 synapses, encountered in five WT and five DAKO cortices)	7.1 ± 0.8	10.8 ± 0.8	0.002
Nonperforated synapses Spine width (nm)	451 ± 18 nm (n = 174)	443 ± 13 nm (n = 320)	0.982
Nonperforated synapses PSD width (nm)	254 ± 8 nm (n = 214)	249 ± 6 nm (n = 408)	0.975
Perforated synapses Spine width (nm)	705 ± 49 nm (n = 24)	682 ± 26 nm (n = 70)	0.978
Perforated synapses PSD width (nm)	523 ± 22 nm (n = 31)	482 ± 13 nm (n = 88)	0.376

ness of the PSD in its plane of section or within the synaptic cleft. Labeling that occurred within the spine head but removed from the PSD by a distance greater than the thickness of the PSD was categorized as occurring "within the spine but not at or near the synapse" (i.e., "nonsynaptic"). For all three immunolabels (HRP-DAB, SIG, and PEG), labeling on the presynaptic side was also categorized as being "at the presynaptic membrane" or "near the presynaptic membrane" or "within the axon terminal but removed from the presynaptic membrane."

The images used to determine NR2A immunoreactivity were reanalyzed to determine the density of synapses in layer 1 of cortex. Frequency of encounter with synaptic profile was determined by calculating the mean of the number of synaptic profile encountered in each electron micrograph spanning a synaptic neuropil area equal to 29 μm^2 and free of blood vessels, somata, and large dendritic shafts (Table 2). For estimating the density of synapses per unit volume, the Abercrombie correction was applied, using the following formula:

$$N_v = N_A[T/(T + d)],$$

where N_v = corrected estimate of object number per unit of volume (numerical density), N_A = uncorrected profile estimate per unit of area, T = the mean tissue thickness of the section, and d = the mean diameter of the object (Guillery, 2002). To make this estimation, the mean thickness, T, of ultrathin sections was measured, from multiple 29-μm^2 framed images that were acquired with the same digitizing camera, software, and magnification (×40,000) and in which folded portions of the ultrathin sections were included. Image J was used to measure the thickness of folds, from which thicknesses of single layers of ultrathin sections could be derived.

The images used to determine NR2A immunoreactivity were also analyzed to determine whether the synapses appeared perforated or nonperforated. The frequency of perforated synapses, i.e., excitatory synapses with interruptions in the PSDs, was determined for every group of 10 excitatory synapses encountered. An additional two DAKO and one WT tissues that did not undergo the homeostatic plasticity assay were also used to determine the frequency of perforated synapses. The widths of spine and PSD profiles captured in 2-D digitized images from osmium tetroxide-postfixed tissue were used to assess the relative sizes of spines and synapses in DAKO and WT cortices. Tissue immunolabeled for the NR2A subunit and postfixed with osmium tetroxide were also used to compare the widths of PSDs of NR2A-immunolabeled and unlabeled synapses. Image J (U.S. NIH, Bethesda, MD; http://rsb.info.nih.gov/ij) software was used to measure these lengths, as described previously (Fujisawa et al., 2006).

Statistical analyses

All statistical analyses were performed in Statistica (Statsoft) software. When comparing data across the two hemispheres of one animal, Student's *t*-test was used. When comparing data across more than two groups, ANOVA and Tukey's HSD test were used. Significance was accepted $P < 0.05$.

Western blotting

Neocortical homogenates of two 11-week-old DAKO and two WT littermates were prepared with a Teflon-glass homogenizer and ×10 weight-to-volume ratio of SDS sample buffer, consisting of 2% SDS, 5% 2-mercaptoethanol, 10% glycerol, 1 mM EDTA, 40 mM Tris, and 240 mM glycine at pH 8.5 (Laemmli, 1970). The homogenate was then boiled for 5 minutes. Aliquots of whole homogenates were equalized to 100 μg wet weight of cortical tissue/lane), then subjected to SDS-PAGE with 8% polyacrylamide gels. Proteins were transferred to PVDF membranes (Immobilon transfer membrane; Millipore, Bedford, MA), then probed either with the anti-pan-drebrin monoclonal antibody (clone M2F6 hybridoma supernatant, undiluted; Shirao and Obata, 1986), anti-drebrin A-specific polyclonal antibody (DAS2; diluted to 1:500; Aoki et al., 2005; Song et al., 2008), the NR2A antibody (1:1,000 dilution), the anti-NR1 antibody (1:2,000), or the β-actin antibody (1:10,000). After incubation with the HRP-conjugated secondary antibody, immunoreactive signals were visualized on X-ray films (Hyperfilm-ECL; GE Healthcare, Piscataway, NJ) with ECL detection reagents (GE Healthcare).

RESULTS

Ultrastructure of the DAKO cortex

EM-ICC using HRP-DAB as the label revealed that 71% ± 10% of the spines in the WT cortex exhibit immunoreactivity for drebrin A. Immunoreactivity was also present within dendritic shafts and spine necks (Fig. 2A,B). This was as observed earlier for rat cortices (Aoki et al., 2005; Fujisawa et al., 2006). In contrast, immunolabeling for drebrin A was very slight within individual spines of DAKO cortex, with none exhibiting immunolabeling within spines that were comparable in intensity to those seen in WT cortex. Only 18% ± 5% of the spines exhibited any kind of HRP-DAB labeling and these were of very low levels and diffuse (Fig. 2C). These are likely to reflect weak reactivity of this antibody with proteins other than drebrin A.

EM analysis indicated drebrin A KO does not cause any overt ultrastructural changes. No statistically significant difference was detected in the density of axospinous synapses per unit area ($P = 0.4$), the diameter of spine profiles ($P = 0.98$)

or the diameter of PSD profiles ($P = 0.98$; Table 2). Both the DAKO and the WT cortices exhibited perforated synapses that were approximately twice the diameter of nonperforated synapses (Table 2). The widths of the PSDs and spines exhibiting perforated synapses also were not different across genotypes ($P = 0.38$ and 0.98, respectively). However, one notable difference was in the frequency of perforated synapses. Whereas approximately 7% of the excitatory synapses of WT cortices appeared perforated within 2-D digitally captured images, frequency of perforated synapses within the micrographs collected from DAKO cortices (e.g., Fig. 2C) was increased significantly ($P < 0.005$) to 10% (Table 2). The frequency of encounter with particular profiles is influenced by their size and shape (Mouton, 2002). However, because the mean diameter of perforated synapse profiles was not different across the genotypes (Table 2), the increased encounter with perforated synapse profiles within DAKO tissue is likely to reflect an increase in the number of perforated synapses per unit volume. Together, these observations indicate that the genetic deletion of drebrin A may affect the cycling of synapses between larger and smaller ones (Nieto-Sampedro et al., 1982), without interfering with spinogenesis, synapse growth, or synapse stabilization.

Comparisons of spine density and perforated synapse density across the D- vs. L-APV-treated hemispheres of WT cortices revealed no change ($P = 0.311$, ANOVA with post hoc Tukey HSD test). Similarly, spine density across the two hemispheres of DAKO cortices revealed no change ($P = 0.976$). These findings indicate that 30 minutes of drug application did not induce any net change in the overt aspects of synapse stability.

NR2A immunoreactivity of spines in the cortex of DAKO and WT mice, as revealed by preembed immunolabels

In both the WT and the DAKO cortices, excitatory synapses were identifiable by the presence of thick PSDs on one side (postsynaptic), clustering of small clear vesicles within the profile opposing it (presynaptic), and parallel alignment of the two plasma membranes facing the synaptic cleft. Within spines of WT cortex, HRP-DAB labeling reflecting NR2A immunoreactivity occurred along the postsynaptic plasma membrane. However, most postsynaptic membranes were devoid of HRP-DAB labeling (e.g., "UL PSD" in Fig. 3A–C). Some of those spines lacking NR2A immunoreactivity at the PSD exhibited HRP-DAB at nonsynaptic portions of the spine. The nonsynaptic portions consisted of plasma membranes removed from the synaptic cleft ("NS" in Fig. 3A), intracellular membranes of dendritic shafts (between two arrows in Fig. 3D), and surfaces of the spine apparatus facing the cytoplasm ("sp app" in Fig. 3E,F). These subcellular distribution patterns are in accordance with previous reports of NR2A labeling in the cortex of ferrets (Erisir and Harris, 2003), mice (Kobayashi et al., 2007), and rats (Aoki et al., 2003). NR2A immunoreactivity within spines of DAKO cortices were indistinguishable from the pattern described for the WT brains, in that the labeling was both synaptic (white arrows in Fig. 4) and nonsynaptic (black arrows in Fig. 4).

Although the subcellular distribution of NR2A within spines of DAKO cortices appeared remarkably similar to that of WT cortex, quantitative analysis revealed that the responsiveness of spines to D-APV was strikingly different across genotypes ($P < 0.05$, $t = 2.68$, Student's t-test). After the 30-minute treatment with D-APV, spines in the cortex of WT animals were much more immunoreactive to the NR2A antibody, relative to the synapses in the contralateral hemisphere that received L-APV. Collectively, the interhemispheric comparisons of NR2A immunoreactivity revealed a statistically significant difference for all four WT cortices tested (Fig. 5), the mean of the four values of synaptic NR2A enhancement being 94% ± 28% (mean ± SEM). In contrast, the same analysis of the three DAKO brains revealed no intraanimal, interhemispheric difference (Fig. 5). The degree of enhancement in NR2A immunoreactivity for the DAKO brains was 0% ± 13% (mean ± SEM of the three DAKO brains). There was a trend for the basal levels of synaptic NR2A to be slightly higher within DAKO brains than of WT brains, but this difference across the genotypes did not reach statistical significance. The D-APV-evoked responsiveness that was clearly different across the genotypes indicates that drebrin A is a protein required for the rapid, NMDAR-dependent influx of NR2A-containing NMDARs into spines.

The results obtained from HRP-DAB immunolabeling suggested the D-APV-induced enhancement within spines of WT cortex reflects changes at both the synaptic and the nonsynaptic portions of spines. However, because HRP-DAB labeling is diffusible, precision of antigen localization within spines is limited. To improve the localization of NR2A within spines, we repeated the NR2A immunolabeling using an alternative label, SIG. SIG immunolabeling confirmed that, within spines of WT cortex, NR2A immunolabeling is detectable at synaptic (white arrows in Fig. 6E,G,H) and nonsynaptic (black arrows in Fig. 6F–H) sites. The cortex of DAKO animals also exhibited labeling at synapses (white arrows in Fig. 6A,B) and at nonsynaptic portions within spine heads (black arrows in Fig. 6C,D). Quantitative analysis of three WT brains revealed consistent augmentation of spinous NR2A following the treatment with D-APV, relative to the L-APV-treated cortices (68%, 83%, and 177%). These increments were at synaptic and nonsynaptic sites within spines. In contrast, analysis of two DAKO animals revealed inconsistent, small changes (−4% and 21% relative to control hemispheres).

D-APV effect on spine sizes

Within brains of WT mice, the encounter with NR2A-immunoreactive synapses was more frequent within the D-APV-treated hemispheres than in the contralateral control hemisphere. Although the simplest interpretation of this result is that the proportion of synapses expressing NR2A had increased, another possibility was that the synapses containing NR2A had increased in size following the D-APV treatment. In general, within single, 2-D EM images, processes that are large are encountered more frequently than are the smaller processes, even if they occur in equal numbers (Guillery, 2002; Mouton, 2002). Moreover, although our past experiments had shown that 30 minutes of exposures of the cortex to D-APV does not alter the sizes of asymmetric synapses (Fujisawa et al., 2006), a possibility remained that D-APV enlarges the NR2A-containing synapses specifically. To test for these possibilities, we quantified the relative sizes of asymmetric synapses by measuring PSD widths. This analysis was performed by using sections that had undergone NR2A immunolabeling by the HRP-DAB procedure and postfixation with osmium tetroxide that protected tissue from shrinkage

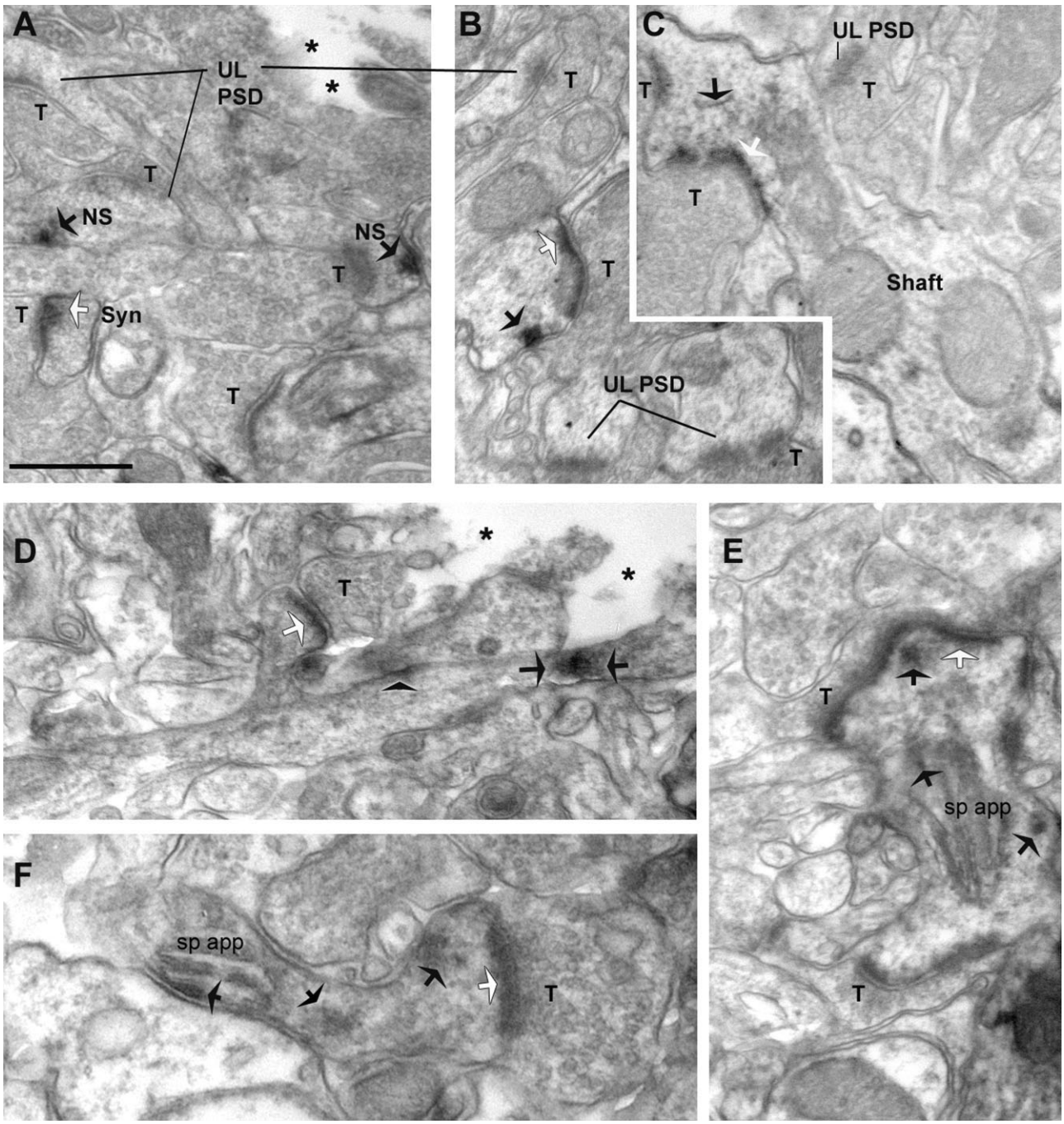

Figure 3.
DAB immunolabeling reveals synaptic and nonsynaptic NR2A within cortical spines of WT mice. Synapses in layer 1 were identified as excitatory, based on the presence of thick postsynaptic densities (PSDs) that align the intracellular surfaces of plasma membranes abutting vesicle-filled axon terminals (T). Asterisks point to portions of the ultrathin sections that are devoid of tissue, indicating the proximity of the sampled region relative to the vibratome surface. **A** was taken from a control hemisphere (L-APV-treated) of WT animal 8, whereas **B–F** were taken from D-APV-treated cortices of two WT animals (animals 6 and 8). In the experimental as well as control hemispheres, NR2A immunolabeling occurs synaptically (white arrows). Immunolabeling is also found at nonsynaptic sites (NS, black arrows) within spines, adjacent to unlabeled PSDs (UL PSD; A), labeled PSDs (B,C,F), and spine apparatus (sp app, in E,F). Yet other HRP-DAB clusters occur removed from spines but are along the plasma membrane of dendritic shafts (arrowhead in D) or reside at sites removed from the plasma membrane in dendritic shafts (between two arrows in D). Scale bar = 500 nm in A (applies to A–E); 688 nm for F.

during tissue processing for EM. We first compared PSD widths of labeled vs. unlabeled synapses. Results of this analysis indicated that NR2A-containing synapses are larger than the unlabeled synapses. Although the synapse width differences were small (49 nm), amounting to a 19% enlargement, relative to the PSD length of unlabeled synapses, these

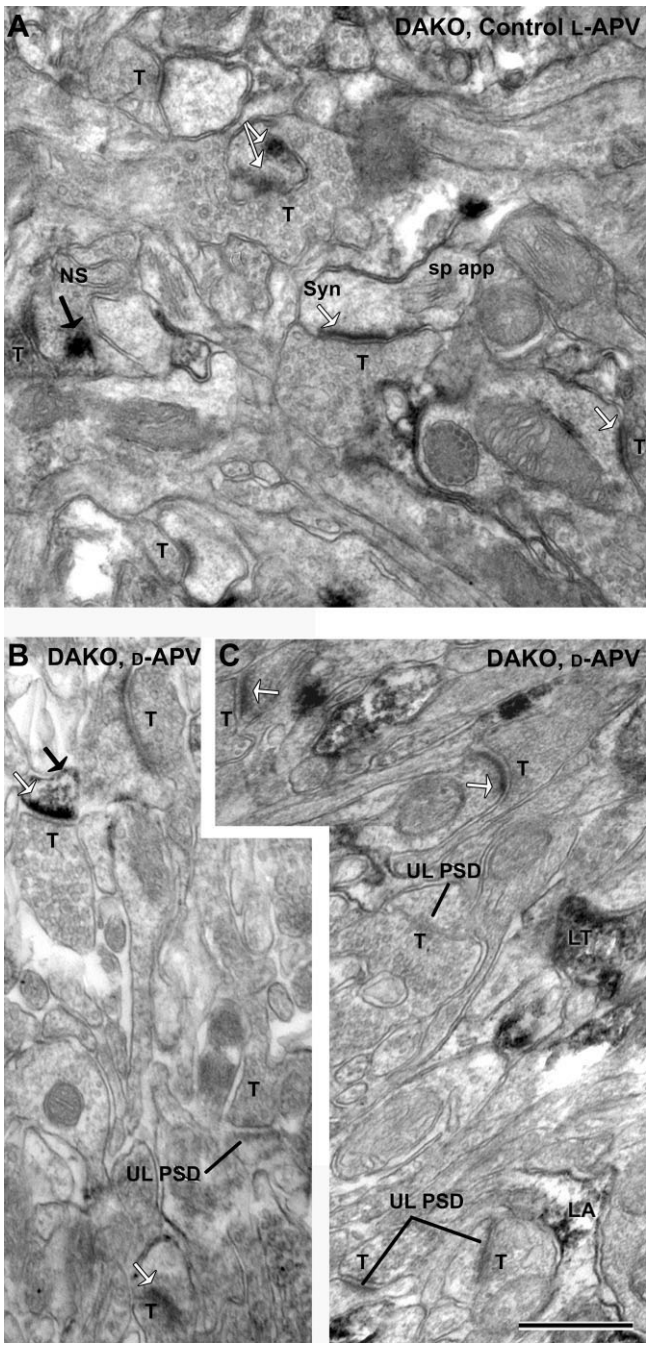

Figure 4.
A–C: DAB labeling of DAKO cortices reveals NR2A labeling at synaptic and nonsynaptic sites within spines. All panels were taken from layer 1 of DAKO animal 9. Synaptic (Syn, white arrows) and nonsynaptic (NS, black arrows) labeling as well as unlabeled PSDs (UL PSD) persist following application of the NMDAR antagonist D-APV. The ultrastructural features of cortical spines and NR2A immunolabeling pattern within dendritic spines are indistinguishable from those of the age-matched WT animals. LT, labeled terminal; T, unlabeled terminal; LA, labeled astrocyte. Scale bar = 500 nm.

differences were highly significant ($P < 0.000001$; t-test, $t = -8.41640$) and consistent across every one of the WT and DAKO brains (not shown).

The synapses encountered from the quantification of NR2A labeling were then separated into eight groups (WT or DAKO; NR2A-labeled or unlabeled; D-APV-treated or control) to obtain the mean values for assessing genotype and drug treatment effects. The mean values were compared by ANOVA and post hoc Tukey's HSD test (df = 2351). Comparisons of PSD widths belonging to labeled vs. unlabeled spines of four WT brains revealed significant differences for both the D-APV-treated hemispheres ($P = 0.00007$) and the control hemispheres ($P = 0.013$). Similarly, comparisons of PSD widths of labeled vs. unlabeled spines of DAKO brains revealed significant differences for both the D-APV-treated hemispheres ($P = 0.0007$) and for the control hemispheres ($P = 0.004$). In sharp contrast to these differences across labeled vs. unlabeled synapses, comparisons of the PSD widths of NR2A-labeled synapses across genotype and drug treatment revealed no difference (Table 3). Specifically, the mean value of PSD widths belonging to NR2A-labeled synapses in the D-APV-treated hemispheres was not significantly different from the mean value of PSD widths belonging to labeled synapses from the control hemispheres, whether compared within WT brains ($P = 0.9999$) or in DAKO brains ($P = 0.947$). These measurements indicated that the apparent increase in encounter with NR2A-labeled synapses in D-APV-treated hemispheres of WT brains is not likely to have resulted from increases in synapse sizes there. Rather, the NR2A levels at synapses and within spines are increased by the D-APV exposure in WT brains, without alterations in the size of synapses. Similarly, the apparent lack of increase of NR2A immunolabeling within the D-APV-treated hemispheres of DAKO brains is not likely to be a result of an actual increase of NR2A immunoreactivity that is counterbalanced by shrinkage of those synapses.

PEG immunolabeling to verify the localization of NR2A subunits at PSDs

The PSD comprises a high density of proteins (Carlin et al., 1980; Kennedy and Ehlers, 2006). Therefore, the apparent absence of responsiveness observed for the DAKO brains might have been due to the inaccessibility of the antibodies to the NR2A subunits that are embedded most deeply in the subsynaptic protein lattice (Bresler et al., 2004). To test for this possibility, we reexamined the synaptic and nonsynaptic population of NR2A using a third EM-ICC procedure, namely, the PEG method, which is a procedure that allows access of antibodies through the deeply embedded proteinaceous matrix. This is achieved by ultrathin sectioning through the PSD. Indeed, the PEG procedure allowed the greatest level of detection of NR2A over the PSD (Fig. 7, graph). However, even by this procedure, DAKO brains (animals 5, 9, and 10; Fig. 7) revealed no D-APV-evoked increase of NR2A immunolabeling, whereas the WT brains responded with robust increases, both at the synapse (animal 6) and at nonsynaptic sites within spines (animal 7). These results confirm that the lack of D-APV-evoked increase of NR2A immunoreactivity within spines of DAKO cortices is not due to failures in the EM-ICC detection of the synaptic population of NR2A subunits. The PEG immunolabeling data confirm that spines of DAKO brains are not responsive to the D-APV treatment. Together, the EM-ICC data demonstrate that DAKO brains are impaired in the rapid form of homeostatic synaptic plasticity.

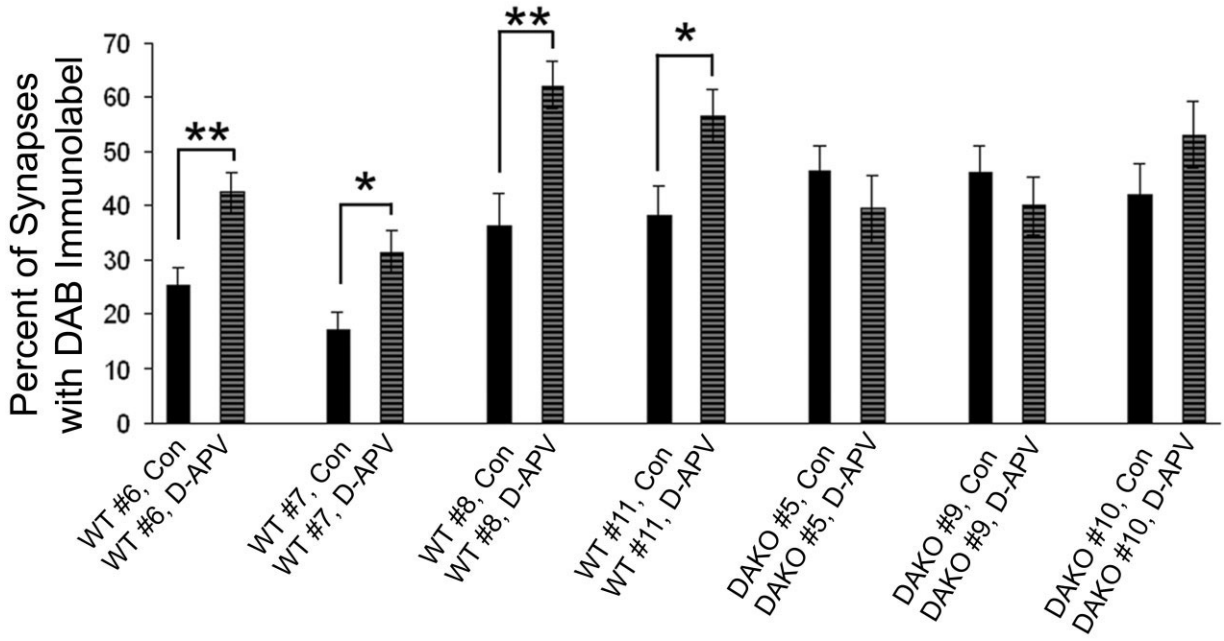

Figure 5.
Quantification of NR2A immunolabeling by HRP-DAB in layer 1 of WT and DAKO brains following 30 minutes of exposure to D- and L-APV. Vibratome sections containing the neocortex of DAKO and WT mice were immunolabeled for the NR2A subunit of NMDARs by the HRP-DAB procedure. For every 10 synapses encountered within layer 1, the proportion with DAB immunulabeling was assessed. This counting procedure was repeated at least 10 times for each hemisphere treated with D-APV and at least another 10 times for the hemisphere that received L-APV. The graph shows the mean value ± SEM of the proportion of spines with immunolabeling. For each of the four WT brains, the proportion immunolabeled for NR2A in the D-APV-treated hemisphere was significantly different from the proportion observed in the L-APV-treated control ("Con") hemisphere (*$P < 0.05$, **$P < 0.005$, comparing across the two hemispheres within animal). None of the brains from the three DAKO animals exhibited differences across the two hemispheres.

DISCUSSION

The application of D-APV upon cortical surfaces of adult WT mice evoked a rapid increase of NR2A immunoreactivity in the spine cytoplasm and at the synaptic junction. This was a response we observed previously for the adult rat cortex. In contrast, neither the synaptic nor the nonsynaptic portions of DAKO spines increased NR2A immunoreactivity following the D-APV blockade. This difference between the genotypes indicates that drebrin A is required for the NMDAR activity-dependent up-regulation of the NR2A subunits within spines and at synapses. Because NR2A subunits form functional heteromers with NR1 subunits before exiting the endoplasmic reticulum (Groc and Choquet, 2006), the elevation of NR2A subunits at synapses is likely to reflect the elevation of NR2A-containing NMDARs at synapses. It has been reported that APV blockade of organotypic hippocampal slices also causes increased influx of NR2A subunits into spines but that the insertion of NR2A subunit-containing receptors into the synaptic membrane requires receptor activation (Barria and Malinow, 2002). Our findings are compatible with this interpretation and indicate that trafficking of NR2A-containing NMDARs to within 10 nm of the synaptic membrane can be accomplished without activation of the NMDARs.

The functions of drebrin A vs. drebrin E

It was a surprise to us that knockout of drebrin A does not affect basal levels of NR2A or the density of spinous profiles. This observation indicates that drebrin A is not required for spinogenesis or synaptogenesis. It is possible that the embryonic isoform of drebrin, drebrin E, which continues to be expressed by DAKO brains, is able to fulfill some of the cellular functions pertaining to the stable structure of spines and synapses. Apparently, the function reserved specifically for drebrin A is to allow the activity-dependent, rapid, and local regulation of glutamate receptor distributions within spines via a mechanism involving exocytosis and endocytosis of vesicles containing NMDARs. The lateral diffusion of NMDARs from extrajunctional plasmalemmal sites to the synaptic junction may also be facilitated by drebrin A, based on our PEG immunolabeling data that revealed an increase of NR2A specifically at PSDs.

We cannot rule out the possibility that the unresponsiveness of DAKO synapses to D-APV is due to the persistence of drebrin E rather than the absence of drebrin A. The drebrin E that persists may interfere with D-APV-induced cellular mechanisms that lead to increases in NR2A expression levels at synapses. However, we favor the former interpretation. Cultured hippocampal neurons that are grown in vitro for 21 days exhibit the APV-evoked up-regulation of NR1 subunits into spines, even though approximately half of the total drebrin expressed by these neurons is the drebrin E isoform (Takahashi et al., 2006). This indicates that drebrin E does not interfere with the cellular mechanisms that lead to the up-regulation of NMDARs into spines. At the very least, if drebrin

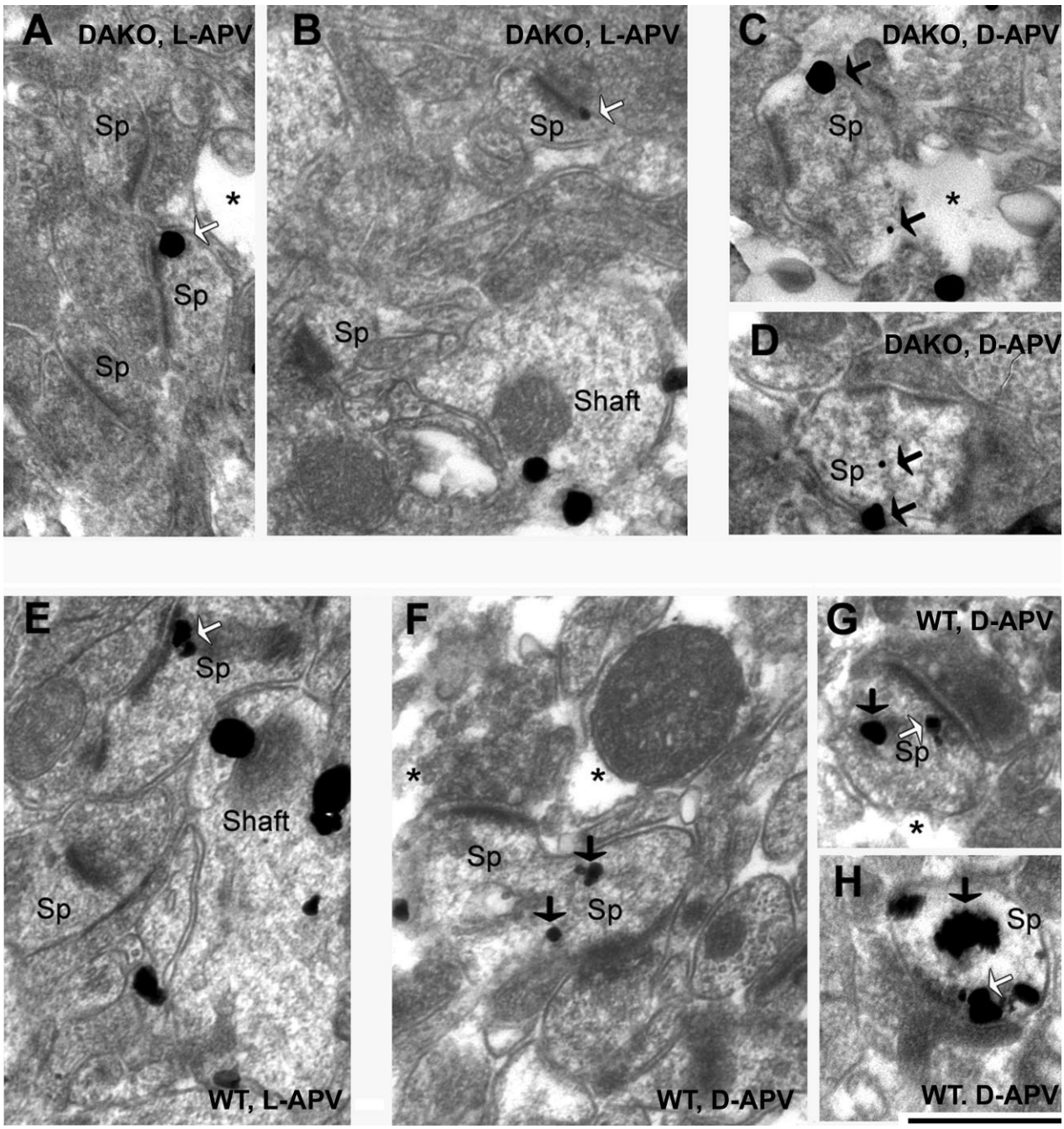

Figure 6.
A–H: SIG labeling confirms similarity in the localization of NR2A. The SIG procedure was employed to be able to distinguish spines with labeling in the vicinity of the postsynaptic membrane vs. those removed from the postsynaptic membrane. DAKO tissue shown here were obtained from animal 10, whereas the WT tissues shown here are from animal 11. SIG occurs at the PSD (white arrows) and removed from the PSD but still within the dendritic spine (Sp, black arrows). Yet others are found in the dendritic shaft, removed from the plasma membrane (Shaft, B,E). Asterisks indicate portions of ultrathin sections that are devoid of tissue, confirming that the sampling is at the surface-most portions of the vibratome section. Scale bar = 500 nm.

E does interfere with homeostatic synaptic plasticity, this inhibitory effect is not sufficiently strong to override the facilitatory role played by drebrin A. Western blot analyses indicate that, at ages younger than P21, intact cortex also exhibits a mixture of drebrin E and drebrin A (Aoki et al., 2005). Assuming that the Western blot result reflects individual neurons expressing a mixture of drebrin E and drebrin A, these neurons are also likely to be able to exhibit the drebrin A-dependent rapid homeostatic synaptic plasticity.

TABLE 3. PSD Width Comparisons (Mean ± SEM)

Labeled 307 ± 5	Unlabeled 259 ± 4	$P = 0.00001$
Genotype effects		
APV-treated labeled WT 297 ± 7	APV-treated labeled DAKO 315 ± 10	$P = 0.826$
Control labeled WT 294 ± 11	Control labeled DAKO 331 ± 10	$P = 0.146$
APV-treated unlabeled WT 249 ± 7	APV-treated unlabeled DAKO 263 ± 7	$P = 0.830$
Control unlabeled WT 250 ± 7	Control unlabeled DAKO 282 ± 9	$P = 0.084$
Pharmacological treatment effects		
APV-treated labeled WT 297 ± 7	Control labeled WT 294 ± 11	$P = 0.999$
APV-treated labeled DAKO 315 ± 10	Control labeled DAKO 331 ± 10	$P = 0.947$
APV-treated unlabeled WT 249 ± 7	Control unlabeled WT 250 ± 7	$P = 1.000$
APV-treated unlabeled DAKO 263 ± 7	Control unlabeled DAKO 282 ± 9	$P = 0.683$

Methodological considerations

We observed some interanimal differences in basal levels of NR2A within spines. We were able, regardless of these differences, to detect differences in the D-APV responses across genotypes by making homeostatic synaptic plasticity measurements that relied on intraanimal, interhemispheric measurements for comparing single brain's reactivity to the D- vs. L-APV.

We cannot rule out the possibility that the differences in baseline levels arose post-mortem, because of differences in the treatment of brain sections. However, we think that the post-mortem introduction of artifacts was minimized to the limit of the methodology, because considerable effort was put into treating the brains uniformly. For example, transcardial perfusion of animals used the same peristaltic pump, set at a single flow rate and perfusate volume. The post-perfusion fixation period was set to 5 hours, by using sodium borohydride to control the termination point of tissue fixation. Finally, all tissue underwent the same steps of EM-ICC, in parallel.

On the other hand, what we observed may actually reflect inter-animal variability in behavior and synaptic structure, even though the animals were derived from a single strain and genotype. It has been shown that rats from a single strain and breeding colony exhibit a wide range of fear reactivity, as is measured by the number of seconds that the animals freeze to a conditioned tone following fear conditioning (Bush et al., 2007). Whether such behavioral differences reflect quantitative differences in receptor density at synapses within discrete regions of the brain remains to be explored. Also, these animals underwent a somewhat unusual rearing environment, consisting of the vivarium in Japan and the United States as well as an intercontinental shipment experience and group housing. The experiences that these mice received during the 3 postnatal months might have contributed to inter-animal variability.

Mechanism underlying the rapid rise of NR2A in spines and at synaptic junctions

Another in vivo assay revealed that the NR2B-to-NR2A switching of NMDAR subunits can occur rapidly (within 1 hour, but no less than 30 minutes) in the visual cortex, following the initial exposure of developing rodents to visual stimulus (Quinlan et al., 1999). Such a delay may be due to the need for the sequential events involving transcription, translation and finally trafficking of the newly synthesized proteins to critical sites to allow trafficking of NR2A subunits. Although 1 hour is a delay sufficiently long to evoke transcriptional mechanisms, whether or not transcriptional mechanisms can account for the augmentation of the NR2A-containing NMDARs that we observed within the first *half* hour remains to be tested. Even Arc, one of the immediate early genes that can be induced by neural activity and is thought to play a role in receptor trafficking, exhibits a delay of about 2 hours before the proteins rise to levels detectable within stimulated regions of the brain (Ploski et al., 2008). On the other hand, insofar as Arc mRNA can reside near spine necks (Bramham, 2008), it is possible that the newly synthesized Arc protein facilitates the trafficking of NMDARs to the synaptic junction within 30 minutes of receptor blockade. Because we have no reason to suspect that Arc-mRNA levels are affected by DAKO, the loss of the rapid response observed within DAKO cortices indicates that drebrin A is at least as important as Arc in the activity-dependent redistribution of NMDARs to synapses. If NMDAR subunit mRNAs already reside in the vicinity of spine heads, such as the parent dendritic shaft (Martin and Zukin, 2006), then it is possible that NR2A mRNA trafficking toward spine heads and a highly localized de novo synthesis of NR2A subunits also contribute to the rise of NR2A immunoreactivity within spine heads and at the synaptic junction. A decrease in NR2A proteolysis may also have contributed to the rise in immunoreactivity at synapses. In summary, the rapidity with which the excitatory synapses responded in the current study suggests that the rise of synaptic NR2A immunoreactivity might have occurred without the participation of transcriptional mechanisms, whereas de novo synthesis of proteins and decreased proteolysis, along with the trafficking of already existing receptor proteins to synaptic sites might have contributed to the observed rise.

In healthy brains, long-term sensory deprivation or tetrodotoxin (TTX) blockade of action potentials can lead to compensatory increases in cortical excitability through shifts in the balance of excitatory-to-inhibitory synapses or of the intrinsic excitability of neurons (Kotak et al., 2005; Maffei and Turrigiano, 2008; Sarro et al., 2008). On the other hand, aberrant set points of homeostasis can cause chronic hyperexcitability that leads to illnesses, such as the central pain syndrome, where nonpainful tactile stimuli are perceived as excruciating pain (Wang and Thompson, 2008). Experiments are underway to determine whether DAKO animals exhibit impairment in homeostatic plasticity over a longer time scale and in learning paradigms.

Putative role of F-actin in drebrin A's action

We observed previously that NMDAR blockade leads to an increase of F-actin and drebrin A in spines, together with NR2A, within the first half hour and without evoking overt changes in spine size or density (Aoki et al., 2003; Fujisawa et al., 2006). Similarly, mouse cortex also responds to NMDAR blockade with the rise of NR2A that is unaccompanied by spine size changes. Conversely, activation of glutamate receptors can depolymerize F-actin (Star et al., 2002) and, if intense enough, lead to the collapse of spines (Halpain et al., 1998). Even without activation of glutamate receptors, perturbation of F-actin can lead to the collapse of spines and the loss of synaptic proteins, including a subpopulation of

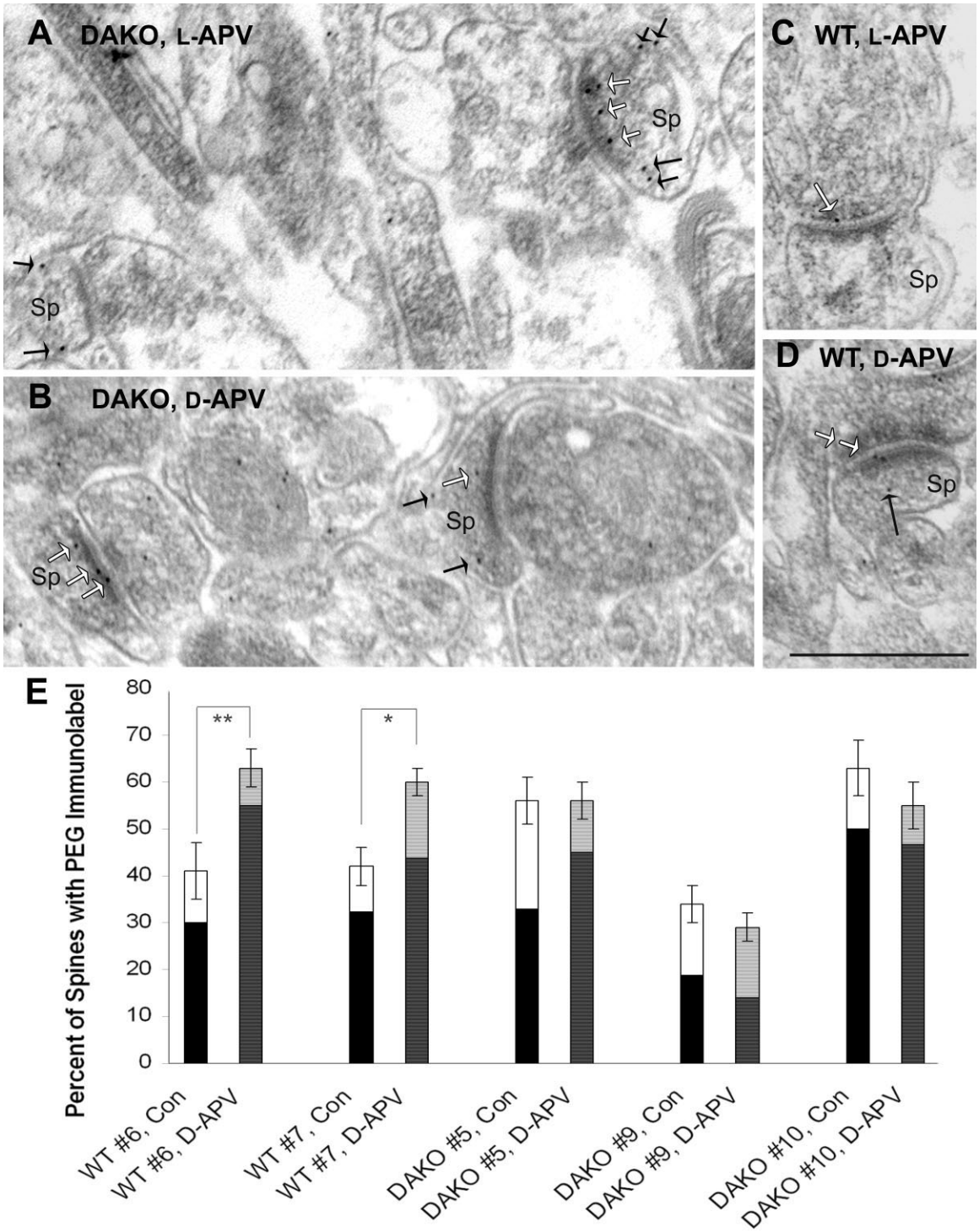

Figure 7.
A–D: PEG labeling reveals the localization of NR2A at and near thick PSDs of both genotypes but responsiveness to NMDAR blockade only within the WT cortex. The PEG procedure was employed to identify the portion of receptor subunits residing precisely over the PSD. Images from DAKO mouse brain were taken from animal 5, whereas the images from WT mouse brain were collected from animal 6. PEG particles are found residing at or near the synapse (white arrow) and also at sites removed from the PSD but still in within dendritic spine (Sp, black arrows). The bar graph (**E**) shows the percentage of spines immunolabeled for the NR2A subunit by the PEG procedure. Comparison of this value between the L-APV (control)- and the D-APV-treated hemispheres of WT brains (animals 6 and 7) reveals an interhemispheric difference in the proportion of spines exhibiting NR2A immunoreactivity over the entire cytoplasm of spines (represented by the total height of bars) and in the immediate vicinity of PSDs (darkened portion of the bars). In contrast, spines of DAKO brains (animals 5, 9, and 10) exhibited no significant difference in the distribution of the NR2A subunits at regions surrounding or removed from PSDs. $^{*}P < 0.05$, $^{**}P < 0.005$. Scale bar = 500 nm.

NMDARs (Allison et al., 1998, 2000). Because NMDARs can be associated with F-actin via α-actinin (Krupp et al., 1999; Wyszynski et al., 1997), NMDAR and other proteins may be anchored to the subsynaptic surface or be liberated from synapses through F-actin dynamics. The F-actin depolymerization experiments also indicate that the F-actin lattice within spines could be serving dual roles, one of anchoring receptors and scaffolding proteins along the postsynaptic membrane facing the synaptic cleft and another for maintaining the overall shape of spines. If this is so, or perhaps particularly because of the dual roles ascribed to F-actin, it remains unclear whether the loss of glutamate receptors at the synapses following receptor stimulation occurs as a consequence of spine collapse or as a consequence of depolymerization of F-actin that is restricted to the subsynaptic membrane surface.

Results from the current study indicate that NR2A levels change independently of spine size changes. Therefore, it is possible that the drebrin A-mediated rise of NR2A immunoreactivity involves liberation of NR2A-containing NMDARs that are tethered in the vicinity of spines, such as the neck and dendritic shaft, via the F-actin lattice there. In support of this idea, we (Fig. 3D) and others (Allison et al., 1998) have observed NMDAR subunit immunoreactivity within dendritic shafts near spine heads, and these have been shown to be tethered to the plasma membrane via F-actin lattices and/or α-actinin. It is also possible that the influx of receptor-containing vesicles into the spine head is facilitated by the influx of drebrin into the spine head that leads to the relaxation of F-actin cross-links formed by α-actinin. Conversely, in the absence of drebrin A, such as in DAKO brains, the entry of receptor-containing vesicles into the spine head and the liberation of NMDARs tethered to F-actin for the subsequent mobilization may be impaired because of the relative rigidity of spine heads and necks.

An increased proportion of perforated synapse: enhanced connectivity but at the expense of plasticity?

One notable structural difference in DAKO cortices was the prevalence of perforated axospinous synapses. Correlative ultrastructural-ICC studies indicate that perforated synapses are particularly efficacious because of the enrichment of AMPA receptors and the large spine head, but without concomitant increases in the number of NMDARs (Kharazia et al., 1996; Nicholson and Geinisman, 2009). Apparently, synapse enlargement does not require the concomitant influx of NMDARs. The prevalence of perforated synapses, together with the similar basal levels of NMDARs found within DAKO spines, indicate that DAKO cortex retains functional synaptic pathways. Whether the perforated synapses of DAKO cortex also exhibit enrichment of AMPARs remains to be tested, but, if they do, the prevalence of perforated synapses within DAKO cortex would suggest that synaptic pathways are strong and stable. On the other hand, the literature on perforated synapses also indicates that these synapses occur at certain immature stages that precede robust synaptogenesis (Nieto-Sampedro et al., 1982) and following episodes of robust synaptic activity, such as epileptic seizure (Henry et al., 2008), cortical stimulation (Adkins et al., 2008), the passive avoidance test (Platano et al., 2008), and water-maze training (Hongpaisan and Alkon, 2007). These are examples of experiences that are likely to evoke synaptogenesis and synapse pruning. The prevalence of perforated synapses within DAKO cortices may reflect the "freezing" of synapse cycling at a stage preceding synapse division (Carlin and Siekevitz, 1983) or pruning, and with it, the loss of mechanisms that ensure synaptic strengths to be self-regulated in ways that mirror sensory experience and synaptic activity.

Is impairment in the activity-dependent NMDAR recruitment causal to the increased incidence of perforated synapses? We do not know. However, one possible scenario is that, in spines of WT cortex, the activity-dependent recruitment of NMDARs can augment the activity-dependent influx of calcium, which in turn promotes severing of F-actin into shorter fragments by the protein gelsolin. These may be the steps allowing spines of WT cortex to cycle between large and small spines and with varying concentrations of AMPARs and NMDARs. Live, in vivo imaging of adult cortices has shown that 5–8% (Zuo et al., 2005) or up to 30% (Holtmaat et al., 2005) of the dendritic spines turn over within 1 month, leaving most of the excitatory synapses stable (Pan and Gan, 2008). A prediction consistent with this idea is that the turnover rate of spines in DAKO cortex will be less than that observed for spines in WT cortex.

Mice with conditional ablation of the β-catenin gene also exhibit elevated frequency of perforated synapses (Bamji et al., 2003), whereas triple knock-in of genes linked to Alzheimer's disease (Bertoni-Freddari et al., 2008) and knockout of the GluR2 subunit of AMPA receptors (Medvedev et al., 2008) exhibit decreased levels of perforated synapses. Both the reduction and the elevation of perforated synapses may reflect impairments in the activity-dependent synapse cycling mechanism. Whether the increased frequency of perforated synapses is associated with the phenotypes of reduced synaptic plasticity, reduced mental capacity, and neurodegeneration is a topic that can be addressed experimentally in future studies that examine the behavior and brain histology of DAKO animals. In support of this idea, we noted that hippocampal spines of an Alzheimer's disease mouse model exhibit reduction of drebrin A and an increase in the mean area of spine head profiles within the hippocampus (Aoki et al., 2007). Brains of patients diagnosed either with AD or mild cognitive impairment also show reduction of drebrin (Counts et al., 2006; Harigaya et al., 1996; Hatanpaa et al., 1999; Shim and Lubec, 2002). Although results of the current study indicated that NMDAR blockade leads to the up-regulation of NMDARs, together with drebrin itself (Fujisawa et al., 2006), previous studies have indicated an opposite effect following NMDAR activation: efflux of drebrin A from spines (Sekino et al., 2006) and PSD-95-regulated endocytosis of NR2A-containing NMDARs from synapses (Sornarajah et al., 2008). Altogether, these findings support the idea that impairment in synapse turnover and synaptic plasticity associated with Alzheimer's disease may be caused, at least in part, by the reduction of drebrin, which leads directly to the loss of bidirectional homeostatic synaptic plasticity, i.e., activity-dependent recruitment of NMDARs into spines or removal of NMDARs out of spines. Loss of this drebrin A-dependent, bidirectional homeostatic synaptic plasticity may ultimately lead to cognitive impairments and excitotoxicity. If so, then manipulations that boost drebrin A levels may be beneficial for enhancing cognitive abilities of patients afflicted by Alzheimer's disease. Although highly speculative, this is a working model that can be tested by examining the consequence of

drebrin A overexpression within mouse models of Alzheimer's disease.

ACKNOWLEDGMENTS

We thank Dr. Sho Fujisawa, Dr. Robert Levy, and Veera Mahadomrongkul for their assistance with the pilot studies. We also thank Dr. Robert Levy, Gerardo Moreno, and Hilda M. Fernandez for their technical assistance and Hermina Nedelescu for reading the manuscript.

LITERATURE CITED

Adkins DL, Hsu JE, Jones TA. 2008. Motor cortical stimulation promotes synaptic plasticity and behavioral improvements following sensorimotor cortex lesions. Exp Neurol 212:14–28.

Aguilar J, Rivadulla C, Soto C, Canedo A. 2003. New corticocuneate cellular mechanisms underlying the modulation of cutaneous ascending transmission in anesthetized cats. J Neurophysiol 89:3328–3339.

Allison DW, Gelfand VI, Spector I, Craig AM. 1998. Role of actin in anchoring postsynaptic receptors in cultured hippocampal neurons: differential attachment of NMDA vs. AMPA receptors. J Neurosci 18: 2423–2436.

Allison DW, Chervin AS, Gelfand VI, Craig AM. 2000. Postsynaptic scaffolds of excitatory and inhibitory synapses in hippocampal neurons: maintenance of core components independent of actin filaments and microtubules. J Neurosci 20:4545–4554.

Aoki C, Rodrigues S, Kurose H. 2000. Use of electron microscopy in the detection of adrenergic receptors. Methods Mol Biol 126:535–563.

Aoki C, Fujisawa S, Mahadomrongkul V, Shah PJ, Nader K, Erisir A. 2003. NMDA receptor blockade in intact adult cortex increases trafficking of NR2A subunits into spines, postsynaptic densities, and axon terminals. Brain Res 963:139–149.

Aoki C, Sekino Y, Hanamura K, Fujisawa S, Mahadomrongkul V, Ren Y, Shirao T. 2005. Drebrin A is a postsynaptic protein that localizes in vivo to the submembranous surface of dendritic sites forming excitatory synapses. J Comp Neurol 483:383–402.

Aoki C, Mahadomrongkul V, Fujisawa S, Habersat R, Shirao T. 2007. Chemical and morphological alterations of spines within the hippocampus and entorhinal cortex precede the onset of Alzheimer's disease pathology in double knock-in mice. J Comp Neurol 505:352–362.

Bamji SX, Shimazu K, Kimes N, Huelsken J, Birchmeier W, Lu B, Reichardt LF. 2003. Role of beta-catenin in synaptic vesicle localization and presynaptic assembly. Neuron 40:719–731.

Barria A, Malinow R. 2002. Subunit-specific NMDA receptor trafficking to synapses. Neuron 35:345–353.

Bear MF, Kleinschmidt A, Gu QA, Singer W. 1990. Disruption of experience-dependent synaptic modifications in striate cortex by infusion of an NMDA receptor antagonist. J Neurosci 10:909–925.

Bertoni-Freddari C, Sensi SL, Giorgetti B, Balietti M, Di Stefano G, Canzoniero LM, Casoli T, Fattoretti P. 2008. Decreased presence of perforated synapses in a triple-transgenic mouse model of Alzheimer's disease. Rejuvenation Res 11:309–313.

Biou V, Brinkhaus H, Malenka RC, Matus A. 2008. Interactions between drebrin and Ras regulate dendritic spine plasticity. Eur J Neurosci 27:2847–2859.

Bramham CR. 2008. Local protein synthesis, actin dynamics, and LTP consolidation. Curr Opin Neurobiol 18:524–531.

Bresler T, Shapira M, Boeckers T, Dresbach T, Futter M, Garner CC, Rosenblum K, Gundelfinger ED, Ziv NE. 2004. Postsynaptic density assembly is fundamentally different from presynaptic active zone assembly. J Neurosci 24:1507–1520.

Broach JR, Guarascio VR, Jayaram M. 1982. Recombination within the yeast plasmid 2mu circle is site-specific. Cell 29:227–234.

Brose N, Huntley GW, Stern-Bach Y, Sharma G, Morrison JH, Heinemann SF. 1994. Differential assembly of coexpressed glutamate receptor subunits in neurons of rat cerebral cortex. J Biol Chem 269:16780–16784.

Bush DE, Sotres-Bayon F, LeDoux JE. 2007. Individual differences in fear: isolating fear reactivity and fear recovery phenotypes. J Trauma Stress 20:413–422.

Calon F, Lim GP, Yang F, Morihara T, Teter B, Ubeda O, Rostaing P, Triller A, Salem N Jr, Ashe KH, Frautschy SA, Cole GM. 2004. Docosahexaenoic acid protects from dendritic pathology in an Alzheimer's disease mouse model. Neuron 43:633–645.

Carlin RK, Siekevitz P. 1983. Plasticity in the central nervous system: do synapses divide? Proc Natl Acad Sci U S A 80:3517–3521.

Carlin RK, Grab DJ, Cohen RS, Siekevitz P. 1980. Isolation and characterization of postsynaptic densities from various brain regions: enrichment of different types of postsynaptic densities. J Cell Biol 86:831–845.

Cline HT, Constantine-Paton M. 1990. NMDA receptor agonist and antagonists alter retinal ganglion cell arbor structure in the developing frog retinotectal projection. J Neurosci 10:1197–1216.

Counts SE, Nadeem M, Lad SP, Wuu J, Mufson EJ. 2006. Differential expression of synaptic proteins in the frontal and temporal cortex of elderly subjects with mild cognitive impairment. J Neuropathol Exp Neurol 65:592–601.

Erisir A, Harris JL. 2003. Decline of the critical period of visual plasticity is concurrent with the reduction of NR2B subunit of the synaptic NMDA receptor in layer 4. J Neurosci 23:5208–5218.

Farb CR, Aoki C, Ledoux JE. 1995. Differential localization of NMDA and AMPA receptor subunits in the lateral and basal nuclei of the amygdala: a light and electron microscopic study. J Comp Neurol 362:86–108.

Fujisawa S, Aoki C. 2003. In vivo blockade of N-methyl-D-aspartate receptors induces rapid trafficking of NR2B subunits away from synapses and out of spines and terminals in adult cortex. Neuroscience 121:51–63.

Fujisawa S, Shirao T, Aoki C. 2006. In vivo, competitive blockade of N-methyl-D-aspartate receptors induces rapid changes in filamentous actin and drebrin A distributions within dendritic spines of adult rat cortex. Neuroscience 140:1177–1187.

Groc L, Choquet D. 2006. AMPA and NMDA glutamate receptor trafficking: multiple roads for reaching and leaving the synapse. Cell Tissue Res 326:423–438.

Guillery RW. 2002. On counting and counting errors. J Comp Neurol 447:1–7.

Halpain S. 2006. They're plastic, but they recycle. Neuron 52:746–748.

Halpain S, Hipolito A, Saffer L. 1998. Regulation of F-actin stability in dendritic spines by glutamate receptors and calcineurin. J Neurosci 18:9835–9844.

Harigaya Y, Shoji M, Shirao T, Hirai S. 1996. Disappearance of actin-binding protein, drebrin, from hippocampal synapses in Alzheimer's disease. J Neurosci Res 43:87–92.

Hatanpaa K, Isaacs KR, Shirao T, Brady DR, Rapoport SI. 1999. Loss of proteins regulating synaptic plasticity in normal aging of the human brain and in Alzheimer disease. J Neuropathol Exp Neurol 58:637–643.

Hayashi K, Ishikawa R, Ye LH, He XL, Takata K, Kohama K, Shirao T. 1996. Modulatory role of drebrin on the cytoskeleton within dendritic spines in the rat cerebral cortex. J Neurosci 16:7161–7170.

Henry LC, Goertzen CD, Lee A, Teskey GC. 2008. Repeated seizures lead to altered skilled behaviour and are associated with more highly efficacious excitatory synapses. Eur J Neurosci 27:2165–2176.

Holtmaat AJ, Trachtenberg JT, Wilbrecht L, Shepherd GM, Zhang X, Knott GW, Svoboda K. 2005. Transient and persistent dendritic spines in the neocortex in vivo. Neuron 45:279–291.

Homanics GE, Ferguson C, Quinlan JJ, Daggett J, Snyder K, Lagenaur C, Mi ZP, Wang XH, Grayson DR, Firestone LL. 1997. Gene knockout of the alpha6 subunit of the gamma-aminobutyric acid type A receptor: lack of effect on responses to ethanol, pentobarbital, and general anesthetics. Mol Pharmacol 51:588–596.

Hongpaisan J, Alkon DL. 2007. A structural basis for enhancement of long-term associative memory in single dendritic spines regulated by PKC. Proc Natl Acad Sci U S A 104:19571–19576.

Jin M, Tanaka S, Sekino Y, Ren Y, Yamazaki H, Kawai-Hirai R, Kojima N, Shirao T. 2002. A novel, brain-specific mouse drebrin: cDNA cloning, chromosomal mapping, genomic structure, expression, and functional characterization. Genomics 79:686–692.

Kawase E, Suemori H, Takahashi N, Okazaki K, Hashimoto K, Nakatsuji N. 1994. Strain difference in establishment of mouse embryonic stem (ES) cell lines. Int J Dev Biol 38:385–390.

Kennedy MJ, Ehlers MD. 2006. Organelles and trafficking machinery for postsynaptic plasticity. Annu Rev Neurosci 29:325–362.

Kharazia VN, Phend KD, Rustioni A, Weinberg RJ. 1996. EM colocalization

of AMPA and NMDA receptor subunits at synapses in rat cerebral cortex. Neurosci Lett 210:37–40.

Kinosian HJ, Newman J, Lincoln B, Selden LA, Gershman LC, Estes JE. 1998. Ca^{2+} regulation of gelsolin activity: binding and severing of F-actin. Biophys J 75:3101–3109.

Kobayashi C, Aoki C, Kojima N, Yamazaki H, Shirao T. 2007. Drebrin a content correlates with spine head size in the adult mouse cerebral cortex. J Comp Neurol 503:618–626.

Kotak VC, Fujisawa S, Lee FA, Karthikeyan O, Aoki C, Sanes DH. 2005. Hearing loss raises excitability in the auditory cortex. J Neurosci 25:3908–3918.

Krupp JJ, Vissel B, Thomas CG, Heinemann SF, Westbrook GL. 1999. Interactions of calmodulin and alpha-actinin with the NR1 subunit modulate Ca^{2+}-dependent inactivation of NMDA receptors. J Neurosci 19:1165–1178.

Laemmli UK. 1970. Cleavage of structural proteins during the assembly of the head of bacteriophage T4. Nature 227:680–685.

Lakso M, Pichel JG, Gorman JR, Sauer B, Okamoto Y, Lee E, Alt FW, Westphal H. 1996. Efficient in vivo manipulation of mouse genomic sequences at the zygote stage. Proc Natl Acad Sci U S A 93:5860–5865.

Maffei A, Turrigiano GG. 2008. Multiple modes of network homeostasis in visual cortical layer 2/3. J Neurosci 28:4377–4384.

Malenka RC, Bear MF. 2004. LTP and LTD: an embarrassment of riches. Neuron 44:5–21.

Malmierca E, Nunez A. 2004. Primary somatosensory cortex modulation of tactile responses in nucleus gracilis cells of rats. Eur J Neurosci 19:1572–1580.

Martin KC, Zukin RS. 2006. RNA trafficking and local protein synthesis in dendrites: an overview. J Neurosci 26:7131–7134.

Medvedev NI, Rodriguez-Arellano JJ, Popov VI, Davies HA, Tigaret CM, Schoepfer R, Stewart MG. 2008. The glutamate receptor 2 subunit controls postsynaptic density complexity and spine shape in the dentate gyrus. Eur J Neurosci 27:315–325.

Miller KD, Chapman B, Stryker MP. 1989. Visual responses in adult cat visual cortex depend on N-methyl-D-aspartate receptors. Proc Natl Acad Sci U S A 86:5183–5187.

Mouton PR. 2002. Principles and practices of unbiased stereology: an introduction for bioscientists. Baltimore: Johns Hopkins University. 214 p.

Nicholson DA, Geinisman Y. 2009. Axospinous synaptic subtype-specific differences in structure, size, ionotropic receptor expression, and connectivity in apical dendritic regions of rat hippocampal CA1 pyramidal neurons. J Comp Neurol 512:399–418.

Nieto-Sampedro M, Hoff SF, Cotman CW. 1982. Perforated postsynaptic densities: probable intermediates in synapse turnover. Proc Natl Acad Sci U S A 79:5718–5722.

Pan F, Gan WB. 2008. Two-photon imaging of dendritic spine development in the mouse cortex. Dev Neurobiol 68:771–778.

Perez-Otano I, Ehlers MD. 2005. Homeostatic plasticity and NMDA receptor trafficking. Trends Neurosci 28:229–238.

Phend KD, Rustioni A, Weinberg RJ. 1995. An osmium-free method of epon embedment that preserves both ultrastructure and antigenicity for postembedding immunocytochemistry. J Histochem Cytochem 43:283–292.

Platano D, Fattoretti P, Balietti M, Giorgetti B, Casoli T, Di Stefano G, Bertoni-Freddari C, Aicardi G. 2008. Synaptic remodeling in hippocampal CA1 region of aged rats correlates with better memory performance in passive avoidance test. Rejuvenation Res 11:341–348.

Ploski JE, Pierre VJ, Smucny J, Park K, Monsey MS, Overeem KA, Schafe GE. 2008. The activity-regulated cytoskeletal-associated protein (Arc/Arg3.1) is required for memory consolidation of pavlovian fear conditioning in the lateral amygdala. J Neurosci 28:12383–12395.

Quinlan EM, Olstein DH, Bear MF. 1999. Bidirectional, experience-dependent regulation of N-methyl-D-aspartate receptor subunit composition in the rat visual cortex during postnatal development. Proc Natl Acad Sci U S A 96:12876–12880.

Rabacchi S, Bailly Y, Delhaye-Bouchaud N, Mariani J. 1992. Involvement of the N-methyl D-aspartate (NMDA) receptor in synapse elimination during cerebellar development. Science 256:1823–1825.

Rao A, Craig AM. 1997. Activity regulates the synaptic localization of the NMDA receptor in hippocampal neurons. Neuron 19:801–812.

Rinaldi T, Kulangara K, Antoniello K, Markram H. 2007. Elevated NMDA receptor levels and enhanced postsynaptic long-term potentiation induced by prenatal exposure to valproic acid. Proc Natl Acad Sci U S A 104:13501–13506.

Sarro EC, Kotak VC, Sanes DH, Aoki C. 2008. Hearing loss alters the subcellular distribution of presynaptic GAD and postsynaptic GABAA receptors in the auditory cortex. Cereb Cortex 18:2855–2867.

Sekino Y, Tanaka S, Hanamura K, Yamazaki H, Sasagawa Y, Xue Y, Hayashi K, Shirao T. 2006. Activation of N-methyl-D-aspartate receptor induces a shift of drebrin distribution: disappearance from dendritic spines and appearance in dendritic shafts. Mol Cell Neurosci 31:493–504.

Shim KS, Lubec G. 2002. Drebrin, a dendritic spine protein, is manifold decreased in brains of patients with Alzheimer's disease and Down syndrome. Neurosci Lett 324:209–212.

Shirao T, Obata K. 1986. Immunochemical homology of 3 developmentally regulated brain proteins and their developmental change in neuronal distribution. Brain Res 394:233–244.

Shirao T, Sekino Y. 2001. Clustering and anchoring mechanisms of molecular constituents of postsynaptic scaffolds in dendritic spines. Neurosci Res 40:1–7.

Shirao T, Kojima N, Obata K. 1992. Cloning of drebrin A and induction of neurite-like processes in drebrin-transfected cells. Neuroreport 3:109–112.

Song M, Kojima N, Hanamura K, Sekino Y, Inoue HK, Mikuni M, Shirao T. 2008. Expression of drebrin E in migrating neuroblasts in adult rat brain: coincidence between drebrin E disappearance from cell body and cessation of migration. Neuroscience 152:670–682.

Sornarajah L, Vasuta OC, Zhang L, Sutton C, Li B, El-Husseini A, Raymond LA. 2008. NMDA receptor desensitization regulated by direct binding to PDZ1–2 domains of PSD-95. J Neurophysiol 99:3052–3062.

Star EN, Kwiatkowski DJ, Murthy VN. 2002. Rapid turnover of actin in dendritic spines and its regulation by activity. Nat Neurosci 5:239–246.

Sternberg N, Hamilton D. 1981. Bacteriophage P1 site-specific recombination. I. Recombination between loxP sites. J Mol Biol 150:467–486.

Takahashi H, Mizui T, Shirao T. 2006. Down-regulation of drebrin A expression suppresses synaptic targeting of NMDA receptors in developing hippocampal neurones. J Neurochem 97(Suppl 1):110–115.

Turrigiano GG. 2008. The self-tuning neuron: synaptic scaling of excitatory synapses. Cell 135:422–435.

Wang G, Thompson SM. 2008. Maladaptive homeostatic plasticity in a rodent model of central pain syndrome: thalamic hyperexcitability after spinothalamic tract lesions. J Neurosci 28:11959–11969.

Wu H, Liu X, Jaenisch R. 1994. Double replacement: strategy for efficient introduction of subtle mutations into the murine *Col1a-1* gene by homologous recombination in embryonic stem cells. Proc Natl Acad Sci U S A 91:2819–2823.

Wyszynski M, Lin J, Rao A, Nigh E, Beggs AH, Craig AM, Sheng M. 1997. Competitive binding of alpha-actinin and calmodulin to the NMDA receptor. Nature 385:439–442.

Zuo Y, Lin A, Chang P, Gan WB. 2005. Development of long-term dendritic spine stability in diverse regions of cerebral cortex. Neuron 46:181–189.